Pseudomonas aeruginosa infection reveals a Caspase-1-dependent neutrophil pyroptosis pathway that restrains damaging Histone release

Rémi Planès[1,¶], Karin Santoni[1,¶], Salimata Bagayoko[1], David Pericat[1], Pierre-Jean Bordignon[1], Audrey Hessel[1], Miriam Pinilla[1], Stephen-Andonai Leon-Icaza[1], Elisabeth Bellard[1], Serge Mazères[1], Rim Abdderrahim[1,2], Emilie Doz-Deblauwe[3], Frances Aylward[1,2], Yoann Rombouts[1], Nathalie Winter[3], Jean-Philippe Girard[1], Odile Burlet-Schiltz[1,2], Christine T.N. Pham[4], Mohamed Lamkanfi[5], Christophe Paget[6], Céline Cougoule[1], Anne Gonzalez-De-Peredo[1,2], Renaud Poincloux[1], Emma Lefrançais[1] & Etienne Meunier[1,#]

[1] Institute of Pharmacology and Structural Biology (IPBS), University of Toulouse, CNRS, Toulouse; France.

[2] Mass Spectrometry facility, Institute of Pharmacology and Structural Biology (IPBS), University of Toulouse, CNRS, Toulouse; France.

[3] INRAE, Université de Tours, ISP, Nouzilly, France.

[4] Division of Rheumatology, Department of Internal Medicine, Washington University School of Medicine, Saint Louis, Missouri 63110, USA.

[5] Department of Internal Medicine and Pediatrics, Ghent University, Ghent, Belgium.

[6] Institut national de la santé et de la recherche médicale, Centre d'Etude des Pathologies Respiratoires, UMR 1100, Tours, France.

[#] Address correspondence to: etienne.meunier@ipbs.fr (EM)

Present Address: Institute of Pharmacology and Structural Biology (IPBS), University of Toulouse, CNRS, Toulouse; France

[¶] These authors contributed equally to this work.

Abstract

Neutrophils mediate essential immune and microbicidal processes. Consequently, to counteract neutrophil attack, pathogens have developed various virulence strategies. Here, we showed that *Pseudomonas aeruginosa* (*P. aeruginosa*) phospholipase ExoU drives pathological NETosis in neutrophils. Surprisingly, inhibition of ExoU activity uncovered a fully functional Caspase-1-driven pyroptosis pathway in neutrophils. Mechanistically, activated NLRC4 inflammasome promoted Caspase-1-dependent Gasdermin-D activation, IL-1β cytokine release and neutrophil pyroptosis. Whereas both pyroptotic and netotic neutrophils released alarmins, only NETosis liberated the destructive DAMPs Histones, which exacerbated *Pseudomonas*-induced mouse lethality. To the contrary, subcortical actin allowed pyroptotic neutrophils to physically limit poisonous inflammation by keeping Histones intracellularly. Finally, mouse models of infection highlighted that both NETosis and neutrophil Caspase-1 contributed to *P. aeruginosa* spreading. Overall, we established the host deleterious consequences of *Pseudomonas*-induced-NETosis but also uncovered an unsuspected ability of neutrophils to undergo Caspase-1-dependent pyroptosis, a process where neutrophils exhibit a self-regulatory function that limit Histone release.

Introduction

Over the last 30 years, non-apoptotic forms of cell death have emerged as crucial processes driving inflammation, host defense against infections but also (auto) inflammatory pathologies (Galluzzi et al., 2018).

Unique among all regulated cell necrosis is the capacity of granulocyte neutrophils to undergo the process of NETosis (Brinkmann et al., 2004). NETosis is an antimicrobial and pro-inflammatory from of cell death that promotes the formation of extracellular web-like structures called Neutrophil Extracellular Traps (NETs) (Brinkmann et al., 2004).

NETosis consists in sequential steps that start with nuclear envelope disintegration, DNA decondensation, cytosolic expansion of DNA and its subsequent expulsion through plasma membrane (Thiam et al., 2020). Completion of DNA decondensation and expulsion requires various cellular effectors. Among them, neutrophil serine proteases (Neutrophil elastase, Cathepsin G, Proteinase 3) or caspase-11 can mediate histone cleavage, which relaxes DNA tension (Chen et al., 2018; Kenny et al., 2017; Knackstedt et al., 2019; Papayannopoulos et al., 2010; Sollberger et al., 2018). In addition, granulocyte-enriched Protein arginine deaminase 4 (PAD4), citrullinates histone-bound DNA, which neutralizes arginine positive charges, thus helping nuclear DNA relaxation and decondensation (Li et al., 2010; Thiama et al., 2020; Wang et al., 2009). Then, decondensed DNA is mixed with the neutrophil cytoplasmic granule content such as NE, CathG, PR3 and Myeloperoxidase (MPO) proteins (Chen et al., 2018; Papayannopoulos et al., 2010; Thiama et al., 2020). Finally, sub-cortical actin network disassembly is required to ensure efficient DNA extrusion through the permeabilized plasma membrane (Neubert et al., 2018; Thiama et al., 2020).

Depending on the initial trigger, various signaling pathways such as calcium fluxes (Kenny et al., 2017; Thiama et al., 2020), necroptosis-associated MLKL phosphorylation (D'Cruz et al., 2018), ROS-induced Neutrophil protease release (Papayannopoulos et al., 2010) or endotoxin-activated caspase-11 (Chen et al., 2018, 2021b; Kovacs et al., 2020) all bring neutrophil into NETosis. Common to both ROS- and caspase-11-dependent NETosis is the requirement of the pyroptosis executioner Gasdermin-D (GSDMD) cleavage by both neutrophil serine and caspase-11 proteases, which triggers neutrophil NETosis (Chen et al., 2018; Sollberger et al., 2018). Specifically, active GSDMD forms a pore on PIP2-enriched domains of the plasma and nuclear membrane of neutrophils, which ensures both IL-1-related

cytokine release (Evavold et al., 2018; Heilig et al., 2018; Tsuchiya et al., 2021; Xia et al., 2021) and osmotic imbalance-induced DNA decondensation and expulsion (Chen et al., 2018; Sollberger et al., 2018). An intriguing feature of neutrophils is that, despite GSDMD activation, they resist canonical inflammasome-induced Caspase-1-dependent cell pyroptosis upon *Salmonella* Typhimurium and *Burkholderia thaïlandensis*-activated NLRC4 inflammasome or upon Nigericin/ATP-mediated NLRP3 inflammasome activation (Chen et al., 2014, 2018; Karmakar et al., 2020; Kovacs et al., 2020).

Although the importance of NETosis in host immunity to infections has been well established (Brinkmann et al., 2004; Chen et al., 2018; Kovacs et al., 2020; Li et al., 2010), NETosis dysregulation also associates to autoimmunity, host tissue damages, aberrant coagulation and thrombus that all contribute to pathology such as sepsis or autoimmune lupus (Apel et al., 2021; Biron et al., 2018; Fuchs et al., 2010; Kahlenberg et al., 2013; Knackstedt et al., 2019; Kumar et al., 2015; Lefrançais et al., 2018; Martinod et al., 2015). Specifically, *P. aeruginosa* bacterial strains that express the necrotizing ExoU phospholipase virulence factor of the patatin-like phospholipase A2 family, promote organ damage-dependent acute respiratory distress syndrome (Bagayoko et al., 2021; Howell et al., 2013; Phillips et al., 2003; Sato et al., 2003). Despite seminal studies underlined that neutrophils constitute one of the primary targets of ExoU (Diaz and Hauser, 2010), their importance in ExoU-driven pathology and the associated molecular mechanisms involved remain elusive. Therefore, in this study, we explored the role of regulated neutrophil necrosis upon *P. aeruginosa* infection and addressed the molecular pathways involved.

Using primary murine and human neutrophils, we showed that ExoU phospholipase activity triggers pathological PAD4-dependent NETosis of neutrophils. In addition, the lack of ExoU expression unveiled a compensatory cell necrosis of neutrophils driven by the canonical inflammasome NLRC4. Specifically, NLRC4-driven neutrophil death led to an incomplete NETosis where neutrophil DNA is decondensed and fills the host cell cytosol but is not expulsed out from the cells. Regarding this, whereas both netotic and pyroptotic neutrophils released HMGB1/2 DAMPs, only NETosis liberated the destructive DAMPs Histones, which contributed to *Pseudomonas*-dependent lethality. To the contrary, pyroptotic neutrophils limited poisonous inflammation by keeping DNA-bound Histones intracellularly thanks to a still assembled subcortical actin cytoskeleton. Finally, both ExoU-induced NETosis and neutrophil caspase-1 played a

pro-microbial role in mice by contributing to *P. aeruginosa* spreading. Overall, we established the host deleterious consequences of *Pseudomonas*-induced-NETosis and -pyroptosis of neutrophils but also uncovered an unsuspected ability of neutrophils to undergo caspase-1-dependent pyroptosis, a process where neutrophils exhibit a self-regulatory function that limit specific DAMP release.

Results

NETs contribute to *Pseudomonas aeruginosa* ExoU-driven pathology

In order to determine if neutrophil might be involved in pathology induced by *exoU*-expressing *P. aeruginosa* (*P. aeruginosa*^{ExoU}), we first monitored for the presence of dying neutrophils in the lungs of infected mice. Using intravital microscopy in lungs from transgenic mice expressing GFP under the granulocyte promoter *MRP8* (MRP8^{GFP}), we observed that *P. aeruginosa*^{ExoU} triggered significant neutrophil death that exhibited extracellular DNA, a feature of NETosis (**Figure 1A, Movie S1**). Related to these observations, we detected increased amounts of netotic markers (MPO/DNA or Histone/DNA complexes) in bronchoalveolar fluids (BALFs) from mice infected with *P. aeruginosa*^{ExoU}, whereas those markers were decreased in mice infected with *P. aeruginosa*^{ExoUS142A}, carrying a catalytically inactivating mutation in *exoU* gene (**Figure 1B**). This suggested to us that neutrophils are important targets of ExoU, and that *P. aeruginosa*^{ExoU}-induced neutrophil death might contribute to pathology. A hallmark of neutrophil NETosis-mediated pathology is the dysregulated release and accumulation of DNA extracellular Traps that promote endothelial and epithelial cell damages. As addition of DNAse-1 allows Neutrophil Extracellular Trap (NET) degradation and elimination, we infected mice with *P. aeruginosa*^{ExoU} or *P. aeruginosa*^{ExoUS142A} in presence or not of DNAse-1 and monitored for mice survival, bacterial loads and NET markers (**Figures 1C, D**). The amount of NET markers in BALs of mice infected with *P. aeruginosa*^{ExoU} were strongly decreased, although we did not detect significant induction of NETs upon infection with *P. aeruginosa*^{ExoUS142A} (**Figure 1C**). As consequence, DNAse-1 treatment improved the survival of *P. aeruginosa*^{ExoU}-infected mice but not the overall bacterial load, suggesting that ExoU-induced NETosis mostly contributes to damage-driven lethal pathology (**Figure 1D**). Altogether, our results suggest that ExoU-induced neutrophil NETosis mostly contributes to *Pseudomonas aeruginosa*-dependent pathology.

ExoU phospholipase activity drives PAD4-dependent NETosis

ExoU exhibits a calcium-independent phospholipase A2 activity that triggers epithelial and macrophage cell necrosis. Therefore, we wondered if ExoU phospholipase activity could regulate neutrophil killing by ExoU. Hence, we infected WT murine bone marrow neutrophils (BMNs) or human blood neutrophils with *P. aeruginosa*^{ExoU} (MOI2) or its isogenic mutant *P. aeruginosa*^{ExoUS142A} (MOI2) in presence or absence of the phospholipase inhibitor MAFP. Pharmacological inhibition or genetic inactivation of ExoU phospholipase activity (ExoU^{S142A}) inhibited ExoU-dependent plasma membrane permeabilization in murine (BMNs) and human blood neutrophils (**Figure 2A**), hence confirming the importance of the ExoU phospholipase activity at promoting neutrophil death.

As we observed NET markers in infected mice (**Figure 1C**), we hypothesized that ExoU-dependent neutrophil death might also promote the generation of NETs. Using scanning electron microscopy, we observed that *P. aeruginosa*^{ExoU} stimulated a strong extracellular DNA release in BMNs, a process inhibited by the use of MAFP (**Figure 2B**). Among others, Histone degradation and DNA citullination are two conserved mechanisms that promote DNA relaxation and delobulation (Thiam et al., 2020). Neutrophil elastase and caspase-11 promote Histone degradation (Chen et al., 2018; Sollberger et al., 2018) and PAD4 triggers Histone citrullination (Li et al., 2010; Thiama et al., 2020; Wang et al., 2009). Therefore, we first explored whether ExoU-induced neutrophil DNA delobulation and release required PAD4-dependent citrullination. We observed that *P. aeruginosa*^{ExoU} induced PAD4-dependent Histone Citrullination (**Figure 2C**). In addition, nuclear delobulation and DNA extrusion were strongly impaired in *Pad4*$^{-/-}$ BMNs, suggesting that PAD4 plays a central function at driving DNA release during *P. aeruginosa*^{ExoU} infection (**Figures 2C, D**).

As PAD4-mediated Histone citrullination requires calcium signaling, a process that can be mediated by membrane pore formation (Chen et al., 2018), we infected BMN neutrophils WT or deficient for various neutrophil NETosis regulators such as GP91 (*GP91phox*$^{-/-}$), Neutrophil Elastase, Cathepsin G, Proteinase 3 (*NE*$^{-/-}$*CatG*$^{-/-}$*Pr3*$^{-/-}$), PAD4 (*Pad4*$^{-/-}$) or Gasdermin D (*GsdmD*$^{-/-}$). *GP91phox*$^{-/-}$, *NE*$^{-/-}$*CatG*$^{-/-}$*Pr3*$^{-/-}$, *Pad4*$^{-/-}$ and *GsdmD*$^{-/-}$ neutrophils all lysed (LDH release) to the same extend (**Figure 2E**). In addition, Scanning Electron Microscopy (SEM) analysis of NET formation showed no differences in the ability of *NE*$^{-/-}$*CatG*$^{-/-}$*Pr3*$^{-/-}$ or *GsdmD*$^{-/-}$ to go into NETosis upon *P. aeruginosa*^{ExoU} whereas *Pad4*$^{-/-}$ showed resistance to trigger NETosis (**Figure 2F**).

This suggested to us that not only ExoU-induced NETosis occurs independently from classical NETotic regulators but also that ExoU-dependent neutrophil lysis could be uncoupled from PAD4-driven DNA decondensation and expulsion (referred here as NETosis). Next, we wondered about the respective importance of neutrophil lysis and PAD4-driven NETosis on the cell-autonomous immune response of neutrophils to *P. aeruginosa*^{ExoU}. We infected WT or *Pad4*$^{-/-}$ BMNs in presence or absence of MAFP and we observed that MAFP-treated neutrophils, but not *Pad4*$^{-/-}$ cells had improved bacterial killing capabilities (**Figure S2A**), hence suggesting that ExoU-mediated neutrophil lysis is sufficient to escape the microbicidal action of neutrophils.

Finally, we noticed that the infection of neutrophils with *P. aeruginosa*^{ExoU} in presence of MAFP only decreased but not abrogated neutrophil plasma membrane permeabilization after 3 hours of infection (**Figure 2G**). In this context, MAFP-treated *GsdmD*$^{-/-}$ neutrophils showed an improved protection upon *P. aeruginosa*^{ExoU}-induced plasma membrane permeabilization (**Figure 2**). Consequently, phospholipase inhibition by MAFP or infection with *P. aeruginosa*^{ExoUS142A} specifically induced Caspase1- and Gasdermin-D-dependent IL1β release although *P. aeruginosa*^{ExoU} triggered few or no IL1β release (**Figure S2B**).

Altogether, our results show that *Pseudomonas aeruginosa*-induced neutrophil lysis requires ExoU phospholipase activity, which subsequently triggers PAD4-dependent DNA citrullination, decondensation and expulsion from neutrophils. In addition, inhibition of ExoU phospholipase activity uncovers a compensatory pathway that drives GasderminD-dependent neutrophil lysis and IL1β release upon *P. aeruginosa* infection.

***ExoU*-deficient *P. aeruginosa* exposes a fully functional NLRC4-Caspase-1-Gasdermin D-dependent pyroptosis axis in neutrophils.**

The observation that, in absence of ExoU phospholipase activity, GSDMD mediates neutrophil death, encouraged us to decipher the molecular mechanisms behind. The infection with *P. aeruginosa*^{ExoUS142A} (MOI2) of WT murine neutrophils or deficient for various inflammasome sensors or signaling components, namely *Aim2*$^{-/-}$, *Nlrp3*$^{-/-}$, *Nlrc4*$^{-/-}$, *Casp11*$^{-/-}$, *Casp1*$^{-/-}$ and *GsdmD*$^{-/-}$ showed that only *Casp1*$^{-/-}$, *GsdmD*$^{-/-}$ and *Nlrc4*$^{-/-}$ BMNs were protected against *P. aeruginosa*^{ExoUS142A}-dependent cell necrosis and IL-1β release (**Figure 3A**). In parallel, we monitored for plasma membrane permeabilization upon infection with *P. aeruginosa*^{ExoUS142A} (MOI2) in WT and *Casp1*$^{-/-}$

BMNs or human blood neutrophils with (**Figures 3B, C**). Consistently, Sytox Green uptake was strongly reduced in *Casp1*$^{-/-}$ BMNs (**Figure 3B**), a process that the Caspase-1 inhibitor Z-YVAD also repressed in human blood neutrophils upon *P. aeruginosa*^{ExoUS142A} infection (**Figure 3C**).

Those observations were paralleled with the detection of Caspase-1 (p20) and Gasdermin-D (p30) processing fragments in WT but not in *Nlrc4*$^{-/-}$ BMNs (**Figure 3D**). *P. aeruginosa* flagellin and rod/needle components from its Type-3 Secretion System (T3SS) trigger NAIP-dependent NLRC4 inflammasome activation in macrophages. Similarly, the use of *P. aeruginosa*$^{ExoU-}$ (deficient for ExoU), *P. aeruginosa*$^{ExoU-FliC-}$ (lacking both ExoU and Flagellin expression) or *P. aeruginosa*$^{ExsA-}$ (lacking T3SS expression) strains showed that neutrophil death occurred in a T3SS and Flagellin-dependent manner (**Figure S3A**). We extended our observations to other ExoU-expressing *P. aeruginosa* (PA14, PA103) strains invalidated or not for ExoU expression. Indeed, infections of WT or *Nlrc4*$^{-/-}$ BMNs with PA14 and PA103 *P. aeruginosa* strains showed that the lack of ExoU expression also triggered NLRC4-dependent pyroptosis in neutrophils (**Figure S3B**). This, suggests that ExoU expression controls the ability of neutrophils to perform NLRC4-dependent pyroptosis. Neutrophils resist NLRC4/Caspase-1-dependent pyroptosis upon *Salmonella* infection (Chen et al., 2014). Hence, to further analyze the specificity of our findings with *P. aeruginosa*$^{ExoU-}$, we next infected WT or *Nlrc4*$^{-/-}$ BMNs with various bacteria (*Shigella flexnerii*, *Chromobacter violaceum*, *Burkholderia thailandensis*) known to trigger a NLRC4 inflammasome response and monitored for cell death and IL-1β release (**Figure 3E**) (Chen et al., 2014; Kovacs et al., 2020; Kumari et al., 2021; Maltez et al., 2015; Zhao et al., 2011). None of the tested bacteria triggered a significant NLRC4-dependent neutrophil lysis although they promoted NLRC4-dependent IL-1β release and gasdermin D processing (**Figures 3E, F**). In contrast to other bacteria, *P. aeruginosa* can use its Type-3 Secretion System independently of its phagocytosis (Hauser and Engel, 1999; Man et al., 2014a). Hence, we hypothesized that in neutrophils, once phagocytosed or endocytosed, bacteria might be exposed to various unknown factors able to restrict the NLRC4 inflammasome response. Regarding this, the direct electroporation of flagellin into the neutrophil host cell cytosol triggered NLRC4-dependent pyroptosis, whereas flagellin transfection, which requires the endocytic pathway to access host cell cytosol, did not lead to detectable neutrophil cell death (**Figure 3G**). This suggests that the route by which NLRC4-activating ligands

are delivered to the cell strongly influences the ability of neutrophils to undergo pyroptosis.

Finally, to determine if *P. aeruginosa*^{ExoUS142A}-induced neutrophil NLRC4 inflammasome activation also occurs *in vivo*, we infected ASC-Citrine mice with low doses (1.10^5 CFUs) of *P. aeruginosa*$^{ExoU-}$ or *P. aeruginosa*$^{ExoU-/FliC-}$, deficient for the expression of Flagellin. ImageStreamX observation of neutrophils presenting an active ASC supramolecular speck (ASC speck$^+$/LY6G$^+$ neutrophils) showed that *P. aeruginosa*$^{ExoU-}$ infection triggered inflammasome activation in neutrophils, which was reduced when mice where infected with *P. aeruginosa*$^{ExoU-/FliC-}$ (**Figure S3C**).

Altogether, our results show that the NLRC4/CASP1/GSDMD axis is fully functional to promote neutrophil pyroptosis in response to *P. aeruginosa* or direct Flagellin electroporation but not to the other NLRC4-activating bacteria tested, suggesting that one or many bacterial virulence or neutrophil intracellular factors might regulate the lytic threshold level of the NLRC4 inflammasome in neutrophils.

Caspase-1-induced neutrophil pyroptosis generates PAD4-dependent intracellular but not extracellular DNA structures

Next, we sought to determine whether Caspase-1-induced neutrophil pyroptosis could also promote NETosis upon *P. aeruginosa*^{ExoUS142A} infection. Scanning electron microscopy experiments showed that Caspase-1- and GasderminD-induced neutrophil pyroptosis did not efficiently generate extracellular DNA structures upon *P. aeruginosa*^{ExoUS142A} infection, although *P. aeruginosa*^{ExoU} robustly induced NETs (**Figure 4A**). Rather, immunofluorescence experiments revealed that *P. aeruginosa*^{ExoUS142A} triggered efficient DNA decondensation as well as expulsion from the nuclear envelop (Lamin-B1 staining) but no or few DNA release from the neutrophil plasma membrane both in murine BMNs and human blood neutrophils (**Figure 4B, S4A**).

Next, we wondered about the mechanisms by which such process might occur. Immunoblotting and microscopy analysis of Histone citrullination showed that *P. aeruginosa*^{ExoUS142A} induced a robust Histone3 (H3)-Citrullination in a NLRC4- and GasderminD-dependent manner (**Figure 4C, S4B**), a process that was also seen in human blood neutrophils (**Figure S4C, D**). Conversely, ASC-Citrine BMNs revealed that NLRC4/CASP1/GSDMD-induced DNA decondensation required PAD4 as pharmacological inhibition of PAD4 (GSK484) abrogated both Histone citrullination as

well as the DNA nuclear release (**Figure 4D, E**). In addition, measure of ASC specks (ASC$^+$), cell lysis (LDH release) and IL-1β release in ASC-Citrine, WT, *Pad4*$^{-/-}$ and *Nlrc4*$^{-/-}$ BMNs highlighted that PAD4 was not involved in *P. aeruginosa*^{ExoUS142A}-induced NLRC4 inflammasome activation (**Figure 4D-F**).

Next, to determine if Caspase-1-induced neutrophil lysis and PAD4-dependent DNA decondensation plays a microbicidal function, we infected WT, *Pad4*$^{-/-}$ and *Nlrc4*$^{-/-}$ BMNs with *P. aeruginosa*^{ExoUS142A} and evaluated their cell-autonomous immune capacities. *Nlrc4*$^{-/-}$ BMNs had improved ability to restrict *P. aeruginosa*^{ExoUS142A} infection than WT and *Pad4*$^{-/-}$ neutrophils (**Figure 4G**). Such results were also observed in human blood neutrophils where only Caspase-1 inhibition (Z-YVAD) but not PAD4 inhibition (GSK484) improved neutrophil-mediated *P. aeruginosa*^{ExoUS142A} killing (**Figure 4G**), suggesting that neutrophil pyroptosis more than PAD4-driven DNA decondensation promotes neutrophil failure to restrict *P. aeruginosa*^{ExoUS142A}.

Finally, in order to determine if neutrophils can undergo Caspase-1-dependent death in mice, we infected MRP8-GFP$^+$ mice and monitored for the granulocyte death features using intravital microscopy (**Figure 4H, Movie S2**). Although necrotic granulocytes exhibited NETotic features (e.g. extracellular DNA) upon exposure to *P. aeruginosa*^{ExoU}, *P. aeruginosa*^{ExoUS142A} infection led to the appearance of swelled-round necrotic granulocytes that exhibited intracellular decondensed DNA, similarly to what we observed *in vitro* (**Figure 4H, Movie S2**). This suggests that upon lung infection, Caspase-1-induced neutrophil pyroptosis is well occurring and displays morphological and immunological distinct characteristics to NETs. All in one, our results describe an original pathway by which NLRC4-induced neutrophil pyroptosis generates PAD4-dependent intracellular but not extracellular DNA structures.

Subcortical actin cytoskeleton limits the release of the damaging DAMPs Histones upon Caspase-1-induced pyroptosis

The observation that Caspase-1-induced neutrophil pyroptosis generates an "incomplete" NETosis brought the questions of what process/effectors determine the ability of DNA to breach or not the plasma membrane and what are the immunological consequences of keeping DNA intracellularly.

To address the first question, we took advantage of a recent study from the Waterman lab that found that stabilizing subcortical filamentous actin with the stabilizing agent jasplakinolide did not abrogate DNA decondensation but rather inhibited DNA

expulsion from the neutrophil upon NETosis inuction (Thiama et al., 2020), an observation that our findings with *P. aeruginosa*^{ExoUS142A} mirror. Hence, we sought to determine the behavior of filamentous actin upon both *P. aeruginosa*^{ExoU}-induced NETosis and *P. aeruginosa*^{ExoUS142A}-induced "incomplete" NETosis. Fluorescence microscopy observations showed that upon infection with *P. aeruginosa*^{ExoU} NETotic neutrophils completely lost F-actin staining as well as the nuclear envelop cytoskeletal protein Lamin-B1 (**Figure 5A**). To the contrary, we observed that subcortical F-actin was condensed close to the plasma membrane upon *P. aeruginosa*^{ExoUS142A}-induced neutrophil pyroptosis (**Figure 5A**). Such observations were also validated when we immunoblotted actin in NETotic and pyroptotic neutrophils (**Figure 5B**). Indeed, we observed a disappearance of actin in NETotic samples, whereas actin was still present in samples from pyroptotic neutrophils (**Figure 5B**). Lamin B1, an essential nuclear envelope cytoskeletal component was found to be strongly cleaved upon *P. aeruginosa*^{ExoU} infection and to a lower extend by *P. aeruginosa*^{ExoUS142A}-induced NLRC4-dependent response, suggesting that alterations of various cytoskeletal components might also account for DNA release from the nucleus (**Figure 5B**) (Knight et al., 2019; Li et al., 2020). As Lamin B1 is mostly involved at regulating nuclear integrity but not extracellular DNA release, we mostly focused on the role of actin degradation and/or F-actin destabilization at regulating DNA-breached plasma membrane of neutrophils. To address this, we infected murine neutrophils with *P. aeruginosa*^{ExoUS142A} and after 2h of infection, a time where the neutrophil DNA was decondensed and could fill the intracellular compartment, we added the actin depolymerizing agent Latrunculin A and monitored for the formation of NETs (**Figure 5C**). We controlled that Latrunculin A use did not modify *P. aeruginosa*^{ExoUS142A}-induced neutrophil lysis (LDH release) or ASC supramolecular complexes formation (%ASC specks^{+} cells) (**Figure 5C, S5A**). We observed that Latrunculin A-depolymerized F-actin induced the appearance of NET-like structures in *P. aeruginosa*^{ExoUS142A}-infected neutrophils (**Figure 5C**). To challenge these findings, we also reasoned that if actin depolymerization could induce DNA expulsion upon pyroptosis, actin stabilization might inhibit DNA expulsion upon NETosis induction. In this context, we infected neutrophils with *P. aeruginosa*^{ExoU} for 30 minutes as ExoU triggers a very fast neutrophil NETosis and then added the stabilizing agent jasplakinolide (**Figure S5B**). Microscopy observation and quantification of DNA able to

cross the plasma membrane showed that jasplakinolide-treated cells kept intracellularly their decondensed DNA upon *P. aeruginosa*^{ExoU} infection (**Figure S5B**). These results suggest that cortical F-actin acts as a physical barrier against DNA expulsion upon neutrophil pyroptosis, a capacity that disappears in NETosis contexts. Next, we addressed the immunological relevance of pyroptotic neutrophils. We hypothesized that, contrary to NETs, pyroptotic neutrophils might keep intracellularly several DAMPs in order to lower unnecessary tissue damages.

Subsequently, to determine to what extent the content of released protein might vary between neutrophil pyroptosis and NETosis, we performed a comparative mass spectrometry analysis of the secretomes of pyroptotic and NETotic neutrophils (**Figure 5D**). To ensure a clear comparison, we set up experimental conditions where both NETotic and pytopotic neutrophils died to the same extend (**Figure 5D**). Hence, BMNs were infected for 3 hours with *P. aeruginosa*^{ExoU} at a MOI of 0.5 and *P. aeruginosa*^{ExoUS142A} at an MOI of 2. Comparative analysis of supernatants detected approximatively 450 proteins that were mostly enriched extracellularly (more than two fold) upon NETosis, including Histones core components (Histone H3) or Histone-associated proteins (Histone H1) (**Figure 5D, Table S1**). To the contrary, both pyroptotic and NETotic neutrophils released the necrotic markers Ldh or the alarmins IL36γ, HMGB1 and HMGB2 (Henry et al., 2016; Phulphagar et al., 2021) to a similar extend, suggesting that pyroptosis of neutrophils might interfere with the release of specific DAMPs (**Figure 5D**). These features were then further validated by immunoblotting and ELISA against HMGB1 or Histones release upon both NETosis and pyroptosis induction (**Figures 5E, S5C, D**). In those experiments, only *P. aeruginosa*^{ExoU} promoted strong Histone H3 and Citrullinated Histone H3 release although HMGB1 DAMP was released in both situations (**Figures 5E, S5C, D**). In addition, we observed that latrunculin A-destabilized F-actin also induced Histone 3 release upon *P. aeruginosa*^{ExoUS142A} infection of neutrophils (**Figure 5F**). To the contrary, japlakinoloide strongly impaired ExoU-dependent release of extracellular Histones (**Figure 5F**), hence suggesting that F-actin integrity contributes to restrain DNA-associated Histone release upon neutrophil pyroptosis. When present extracellularly, Histones are extremely potent pro-inflammatory and damaging molecules (Silvestre-Roig et al., 2019; Xu et al., 2009, 2015). Indeed, direct injection of Histones into the blood stream of mice triggers a sepsis like response (Xu et al., 2009). In this context, we hypothesized that *P. aeruginosa*^{ExoU}-induced extracellular

release of Histones might be an important contributor of lethality *in vivo*. Therefore, we infected mice intranasally with *P. aeruginosa*^{ExoU} or *P. aeruginosa*^{ExoUS142A} in presence or absence of N-Acetyl Heparin (NAH), a non-anticoagulant heparin-derived molecule that inhibits Histone mediated cellular damages (**Figures 5G, S5E**) (Wen et al., 2016; Wildhagen et al., 2014; Zhang et al., 2014). *P. aeruginosa*^{ExoUS142A}-infected mice exhibited moderate lethality, which was not significantly modified by the use of NAH (**Figure 5G**). By contrast, NAH strongly improved survival of *P. aeruginosa*^{ExoU}-infected mice, hence suggesting that NETosis specifically contributes to Histone-associated lethality in response to *P. aeruginosa*^{ExoU} (**Figure 5G**).

Altogether, our results unveil an original process where F-actin act as physical barrier able to inhibit DNA extrusion out from neutrophils upon Caspase-1-induced pyroptosis, hence limiting Histone-mediated lethality.

Targeting both inflammasome and ExoU phospholipase activity synergistically improves *P. aeruginosa* elimination.

Our results showed that both NETosis and neutrophil pyroptosis are inefficient at eliminating *P. aeruginosa in vitro* and that NETosis-induced Histone release contributes to *P. aeruginosa*^{ExoU}-driven mouse lethality. In this context, we aimed at determining the role of the Neutrophil Caspase-1 upon *P. aeruginosa* infection in mice. We infected MRP8^{Cre-}*Casp1*^{flox} and MRP8^{Cre+}*Casp1*^{flox} mice either intranasally or systemically with *P. aeruginosa*^{ExoU} or *P. aeruginosa*^{ExoUS142A} strains. We observed that, upon lung and systemic infections with *P. aeruginosa*^{ExoU}, MRP8^{Cre+}*Casp1*^{flox} mice did not show any differences in bacterial elimination, IL1β production or Histone/DNA complexes presence in BALs or plasma, confirming that *P. aeruginosa*^{ExoU} triggers successful infection independently of the inflammasome pathways (**Figures 6A-D, S6A**). To the contrary, MRP8^{Cre+}*Casp1*^{flox} mice infected with *P. aeruginosa*^{ExoUS142A} showed a slight but significant improved bacterial elimination in lungs, a phenotype that was further amplified in systemic infection as shown in spleen, liver and lung (**Figure 6A, C**). In parallel, BAL and plasma IL-1β levels, but not Histone/DNA complexes, were decreased in MRP8^{Cre+}*Casp1*^{flox}, hence suggesting that neutrophil Caspase-1 is also a contributor of IL-1β production upon *P. aeruginosa*^{ExoUS142A} infection (**Figure 6B, D**).

Finally, we aimed at determining if targeting both ExoU phospholipase activity and inflammasome response could synergistically protect mice against infection. Both

Faure et al and Cohen et al previously showed that NLRC4 in macrophages played a deleterious immune response to *P. aeruginosa* lung infection (Cohen and Prince, 2013; Faure et al., 2014). Hence, as NLRC4 in macrophages and neutrophils is of importance in *P. aeruginosa* infection, we infected WT or *Nlrc4*$^{-/-}$ mice with *P. aeruginosa*^{ExoU} or *P. aeruginosa*^{ExoUS142A} and monitored for mice survival and bacterial loads (**FigsS6B, C**). We observed that NLRC4 did not protect against *P. aeruginosa*^{ExoU}-induced lethality or against bacterial growth (**FigsS6B, C**). However, *P. aeruginosa*^{ExoUS142A} infection was strongly attenuated in WT mice, a process that was even further amplified in *Nlrc4*$^{-/-}$ mice that almost entirely cleared bacteria from the lung, hence suggesting that targeting both ExoU-induced lethal pathology and inflammasome-promoted bacterial growth synergistically improve both mice survival and *Pseudomonas* elimination. Altogether, our results highlight that neutrophil Caspase-1 activity contributes to *P. aeruginosa* spreading in mice in absence of ExoU.

Discussion

Induction of NETosis is a crucial process in the host defense against extra- and intra-cellular pathogens but its dysregulation also favors autoimmunity or infectious sepsis. Whereas infections involving *P. aeruginosa* are mostly studied through the chronic prism, which occurs with *P. aeruginosa* strains that initially express (then repress during the chronic infectious stage) the ExoS toxin, ExoU-expressing *P. aeruginosa* strains drive acute and lethal infections (Ozer et al., 2019). Here, we found that upon *P. aeruginosa*^{ExoU} infection, neutrophils undergo pathological NETosis, which induces both aberrant NETosis-induced lethality and bacterial escape from neutrophil uptake and killing. Specifically, ExoU induces phospholipid cleavage and degradation, which triggers neutrophil lysis. Subsequently, neutrophil membrane alterations trigger PAD4 activation, hence ensuring DNA relaxation and the full NETosis process. Although NE/PR3/CathG, ROS and Caspase-11 all play a strong role at promoting NETosis in various infectious and sterile contexts (Chen et al., 2018; Kenny et al., 2017; Papayannopoulos et al., 2010), none of them was important for ExoU-induced neutrophil lysis or NETosis, which suggests that additional factors might control ExoU-induced neutrophil lysis.

A key observation of our study was that, although neutrophils resist NLRC4- and NLRP3-induced Caspase-1-dependent pyroptosis upon various bacterial challenges (Chen et al., 2014; Karmakar et al., 2020; Kovacs et al., 2020), the lack of ExoU

expression induced neutrophil pyroptosis through the engagement of the fully competent canonical NLRC4 inflammasome (Sutterwala et al., 2007). In agreement with previous studies, we did not find another bacterium among the well-known bacteria that trigger NLRC4 inflammasome response able to trigger neutrophil pyroptosis in neutrophils, at the exception of the various strains of *P. aeruginosa* tested. It is clear enough that neutrophils show more resistance than macrophages to NLRC4-dependent pyroptosis (Chen et al., 2014; Heilig et al., 2018; Nichols et al., 2017), yet *P. aeruginosa*^{EXOUS142A} still trigger neutrophil pyroptosis. This suggests to us that beyond their intrinsic resistance to pyroptosis (e.g. ESCRT machinery, Caspase-1 expression levels, Ragulator pathway…) (Bjanes et al., 2021; Chen et al., 2018; Evavold et al., 2020; Rühl et al., 2018), neutrophils might have additional factors that restrict the ability of bacteria to promote NLRC4-dependent pyroptosis. Related to this, a seminal study from Zynchlynsky and colleagues found that neutrophil serine proteases could degrade the Type-3 Secretion System and flagellin virulence factors of *S. flexneri* (Weinrauch et al., 2002), hence limiting their ability to hijack the neutrophil autonomous immunity and restraining *Shigella*-induced neutrophil necrosis. Similarly, upon *P. aeruginosa* infection, neutrophils deficient for the Nadph oxidase enzyme Nox2 undergo some low degree of caspase-1-dependent pyroptosis, which drives a deleterious response of the host (Ryu et al., 2017). As *P. aeruginosa* can inject flagellin directly through the plasma membrane in absence of phagocytosis, one could speculate that bypassing the endocytic/phagocytic pathway of neutrophils, allows escaping T3SS and flagellin degradation or ROS-mediated alterations, hence allowing direct access of large amounts of flagellin into the neutrophil cytosol. Related to this, our results show that flagellin electroporation but not its transfection promotes NLRC4-driven neutrophil pyroptosis, hence suggesting that avoiding the endocytosis/phagocytosis pathway might be sufficient to trigger NLRC4-dependent pyroptosis in neutrophils. Interestingly, Chen and colleagues recently found that upon infection with Yersinia, murine neutrophils induce a pyroptotic program that involves virulence-inhibited innate immune sensing, hence promoting RIPK1-induced Caspase 3-dependent Gasdermin E cleavage and activation and neutrophil pyroptosis (Chen et al., 2021a), which also suggests that neutrophil pyroptosis can occur through different molecular pathways.

Similar to ExoU-mediated NETosis, Caspase-1 and Gasdermin-D also promoted PAD4-dependent Histone Citrullination, which stimulated DNA relaxation and release

from the nucleus but not its extracellular expulsion. Why upon ExoU, Caspase-11 (Chen et al., 2018), MLKL (D'Cruz et al., 2018), NADPH (Kenny et al., 2017) or NE/CatG/Pr3 (Papayannopoulos et al., 2010) stimulation but not upon Caspase-1 activation neutrophils generate two different types of DNA structures remains yet to be investigated. Upon Caspase1-induced pyroptosis in neutrophils, a substantial proportion of subcortical actin was still present on its Filamentous form, which in our settings constrained neutrophil DNA intracellularly whereas ExoU-stimulated neutrophils completely lost cellular F-actin network. Similarly, Thiam et al., (Thiama et al., 2020) also observed that F-actin stabilization allowed the formation these peculiar structures upon Ionomycin-induced NETosis. Interestingly, neutrophil elastase has also been shown to degrade actin (Metzler et al., 2014), hence ensuring efficient NETosis induction. This, suggests that extracellular DNA release, the final step of NETosis, might actually be a cell-regulated process involving various, yet to be determined, regulators (Neubert et al., 2018; Thiam et al., 2020). An obvious question lies on both pyroptotic Caspase-11 and necroptotic MLKL proteins and their ability to directly or indirectly induce actin degradation or F-actin destabilization, and whether additional neutrophil components also determine the ability of neutrophil to specifically control extracellular DNA release in this context.

Regarding the immunological purpose of Caspase-1-induced neutrophil pyroptosis, we hypothesize that, mainly due to the broad diversity of inflammasomes, Caspase-1 has more possibilities to be activated than caspase-11. One guess would be that the decondensation of DNA but its conservation into the intracellular space might be a physical mean for neutrophils to trap some intracellular DAMPs, hence avoiding their passive release and a too strong exacerbation of the inflammatory response. Regarding this, our observations that DNA-bound Histones mostly remain trapped intracellularly, but not HMGB1 alarmin, both initially located in the nucleus show that additional regulatory pathways might be involved at promoting HMGB1 release but not Histones upon neutrophil pyroptosis. In the light of the recent discovery from Kayagaky and colleagues on the role for Ninjurin-1 at promoting active cell shrinkage and HMGB1/nucleosome DAMP release downstream of Gasdermin-D pores in macrophages, the use of Ninjurin-1 deficient mice are full of promises in order to determine if neutrophil extracellular vs intracellular DNA can be a mean to trap DAMPs, hence dampening inflammatory and pathological responses (Kayagaki et al., 2021). All in one, our results unveil an unsuspected ability of neutrophils to undergo caspase-

1-dependent pyroptosis which drives an intriguing "incomplete NETosis", hence expanding our understanding of neutrophil death mechanisms and opening novel research areas regarding the immunological importance of such process in various infectious and non-infectious contexts.

ACKNOWLEDGEMENTS

Nlrc4$^{-/-}$ mice were provided by Clare E. Bryant (Man et al., 2014b) and generated by Millenium Pharmaceutical, *GsdmD*$^{-/-}$ mice (Demarco et al., 2020) came from P. Broz (Univ of Lausanne, Switzerland), *Casp11*$^{-/-}$ and *Casp1*$^{-/-}$/ *Casp11*$^{-/-}$ came from B. Py (ENS Lyon, France) and Junying Yuan (Harvard Med School, Boston, USA) (Li et al., 1995; Wang et al., 1998). Virginie Petrilli (ENS Lyon, France) provided *Nlrp3*$^{-/-}$ mice that were generated by Fabio Martinon (Martinon et al., 2006). Christine T N Pham (Washington University, Seattle, USA) generated and provided the *NE*$^{-/-}$/*CatG*$^{-/-}$/*Pr3*$^{-/-}$ mice (Yan et al., 2016), Thomas Henry (CIRI, Lyon, France) provided *ASC*$^{-/-}$ and *AIM2*$^{-/-}$ mice upon agreement with Genentech (San Francisco, Roche, USA) and. ASC-Citrine (#030744) and *Pad4*$^{-/-}$ (#030315) mice came from Jaxson Laboratory (USA) and were generated by Douglas T Golenbock (University of Massachusetts Medical School, USA) and Kerri Mowen (The Scripps Research Institute, USA) respectively. MRP8^{Cre}/*Casp1*^{flox} mice are provided by Natalie Winter (INRAE Tours Nouzilly, France) and were generated by crossing MRP8^{Cre} (Jackson # 021614) mice with *Caspase1*^{flox} mice generated by Mohamed Lamkanfi (Univ. of Ghent, Belgium)(Van Gorp et al., 2016). MRP8^{CreGFP} and mTmG mice were obtained from Jackson laboratories and generated respectively by Emmanuelle Passegue (UCSF, USA) and Liqun Luo, (Stanford University, USA). *Pseudomonas aeruginosa* strains were a kind gift of Ina Attrée (CNRS, Grenoble, France) and Julien Buyck (Univ. of Poitiers, France). Authors also acknowledge the animal facility and Cytometry/microscopy platforms of the INFINITY, CBI and IPBS institutes and particularly Valerie Duplan-Eche for Imagestream acquisition and analysis. This project was funded by grants from the Fonds de Recherche en Santé Respiratoire - Fondation du Souffle to EL, ATIP-Avenir program, FRM "Amorçage Jeunes Equipes" (AJE20151034460) and the ERC (StG INFLAME 804249) to EM, the European Society of Clinical Microbiology and Infectious Diseases (ESCMID, 2020) to RP, Invivogen-

CIFRE collaborative PhD (to MP) and post-doctoral fellowships (to RP), from Mali and Campus France cooperative agencies to SB and of a NIH grant AR073752 to C.TN Pham. The project benefited of support from Labex/Investissements d'Avenir (French Ministry of research) and the Fondation Bettencourt to the IPBS Animal facility infrastructure development and use.

AUTHOR CONTRIBUTIONS

RP and EM designed the experiments. RP, KS and EM wrote the manuscript. RP and KS performed the experiments with the help of SB, DP, PJB, AH, MP, SALI, YR, RA, ED, FA, CC, AGDP, EL, RP. Specifically RP and RP performed SEM experiments, SM, EB and EL set up and performed intravital mouse experiments, RA, FA, YR and AGDP performed mass spectrometry experiments. JPG, OBS, CTNP, ML, NW and CP provided essential reagents, tools and inputs for the conduct of the project. EM, RP and KS supervised the entire study.

CONFLICT OF INTEREST

Authors have no conflict of interest to declare.

Figure legends

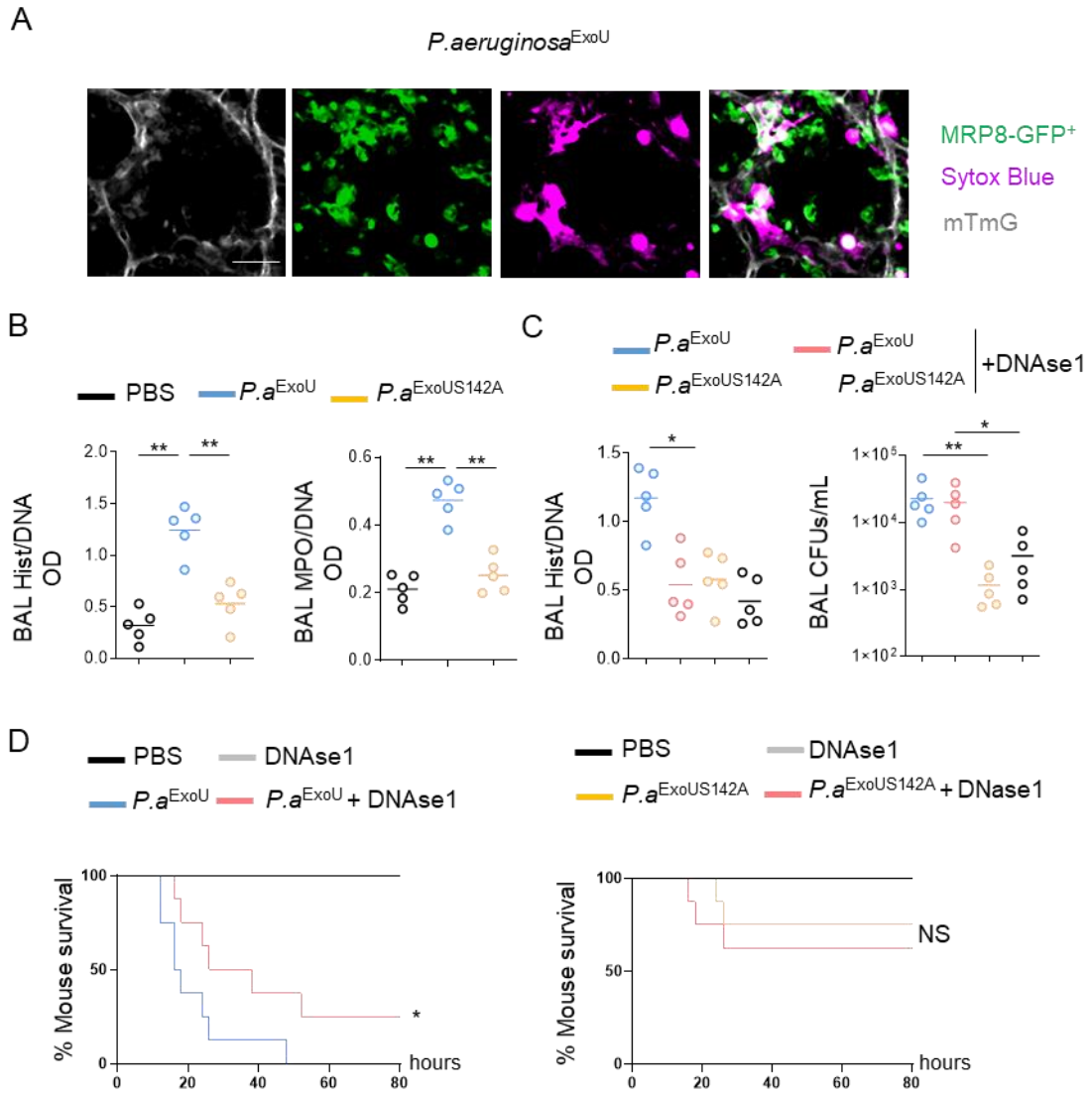

Figure 1. ExoU-dependent NETosis exacerbates pathology induced by *Pseudomonas aeruginosa*.

A. MRP8-GFP^{+} mice were infected with 2.5.10^{5} CFUs of *P. aeruginosa* (*P.a*) expressing *exoU* (*P.a*^{ExoU}) in presence of SYTOX Blue for 10 hours and granulocyte death was observed in infected lungs by the appearance of SYTOX blue fluorescence. Pseudo colors represent vessels (gray, mTG); Granulocytes (Blue, MRP8-GFP^{+}); Dead cells (Yellow, SYTOX blue). Scale bar: 20µm.

B. Histone/DNA and MPO/DNA complexes quantification in Bronchoalveolar Lavages (BALs) from WT mice intranasally infected with 2.5.10^{5} CFUs of *P. a*^{ExoU} or its isogneic mutant expressing a catalytically inactive form of ExoU *P. a*^{ExoUS142A} for 10 hours. Graphs represent one experiment (5 mice/group) out of three independent *in vivo* experiments; **p ≤ 0.01, Mann-Whitney analysis test.

C. BAL bacterial loads (colony forming units, CFUs) and Histone/DNA complexes quantification in WT mice intranasally infected with $2.5.10^5$ CFUs of *P. a*^{ExoU} or *P. a*^{ExoUS142A} for 24 hours. When indicated 4000 unit/mice of DNAse 1, a NET degrading enzyme, were intranasally added both 3 and 9 hours after mice infection. Graphs represent one experiment (5 mice/group) out of three independent *in vivo* experiments; * $p \leq 0.05$, ** $p \leq 0.01$, Mann-Whitney analysis test.

D. Survival of WT mice intranasally infected (n=8 animals per condition) with 5.10^5 CFUs of *P. a*^{ExoU} or *P. a*^{ExoUS142A}. When specified 4000 unit/mice of DNAse 1 were intranasally added 3 and 9 hours after mice infection. Graphs represent one experiment (8 mice/group) out of three independent *in vivo* experiments. Log-rank Cox-Mantel test was used for survival comparisons. * $p \leq 0.05$

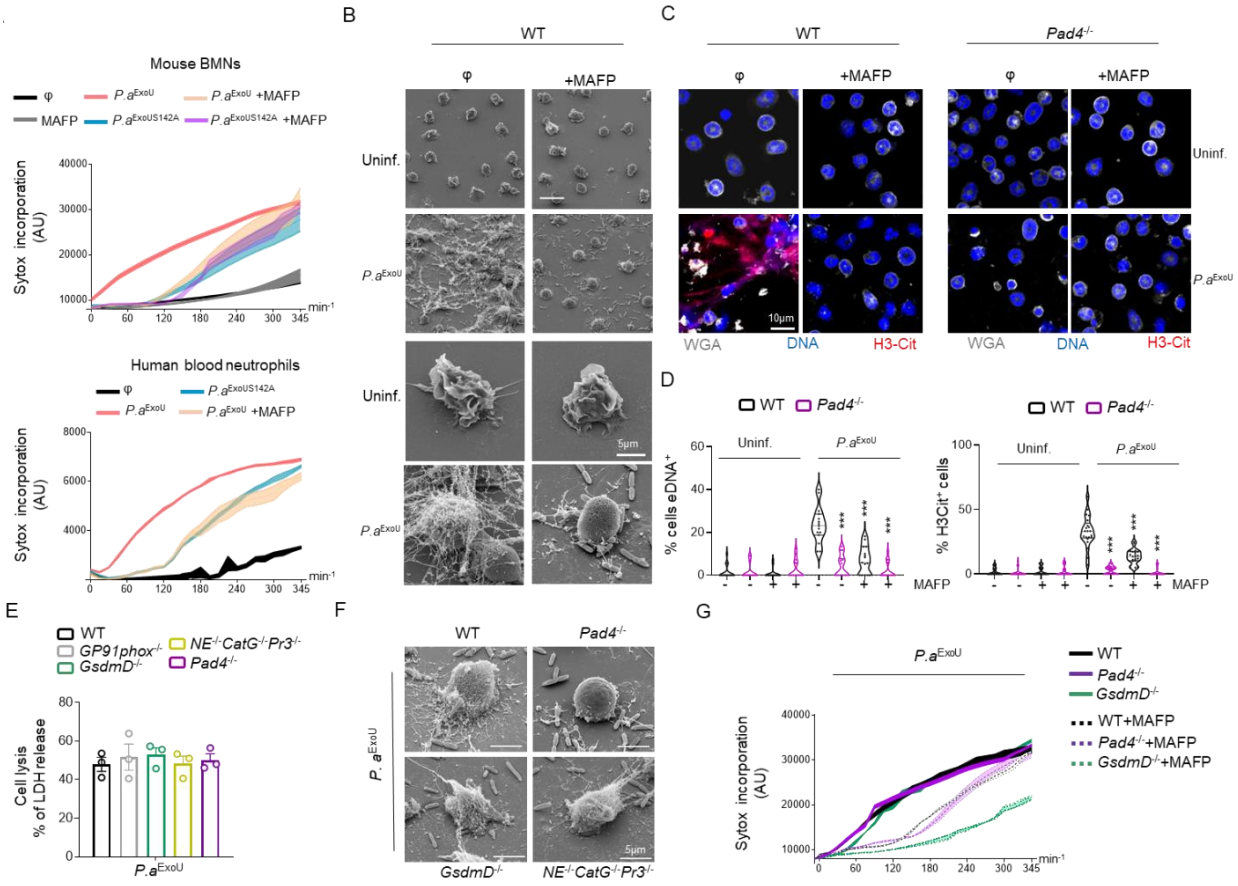

Figure 2. ExoU phospholipase activity triggers NETosis through PAD4-citrullinated Histones.

Otherwise specified, neutrophils were infected with *P. aeruginosa* at a multiplicity of infection (MOI) of 2.

A. Measure of plasma membrane permeabilization over time using Sytox Green incorporation in WT murine Bone Marrow Neutrophils (BMNs) and in human blood neutrophils infected with *P. a*^{ExoU} or *P. a*^{ExoUS142A} in presence or absence of MAFP (20µM), a potent phospholipase activity inhibitor. ***p ≤ 0.001, T-test with Bonferroni correction. Values are expressed as mean ± SEM.

B. Scanning electron microscopy (SEM) observation of BMN NETosis 1h30 after *P. a*^{ExoU} infection in presence/absence of MAFP (20µM).

C, D. Confocal microscopy observation (C) and quantification (D) of Neutrophil Extracellular Traps (NETs) formation in WT or *Pad4*$^{-/-}$ BMNs infected for 1h30 with *P. a*^{ExoU} in presence/absence of MAFP (20µM). Nucleus (blue) was stained with Hoescht; Histone-3 Citrullination is in red (Anti-H3Cit staining); plasma membrane is in grey (WGA staining). Scale bar 10µm. For quantifications, the percentage of cells with extracellular DNA (eDNA^{+}) or positives for H3Cit (H3-Cit^{+}) was determined by

combining the ratios of cells positives for eDNA (outside from plasma membrane) or H3Cit over the total cellular counts from at least 10 fields from n=3 independent experiments. Values are expressed as mean ± SEM.

E. Measure of cell lysis (release of LDH) in WT, *GP91phox*$^{-/-}$, *GsdmD*$^{-/-}$, *NE*$^{-/-}$/*CatG*$^{-/-}$/*Pr3*$^{-/-}$ and *Pad4*$^{-/-}$ BMNs infected for 3 hours with *P. a*^{ExoU}. ***p ≤ 0.001, T-test with Bonferroni correction.

F. Scanning electron microscopy (SEM) observation of NETosis in WT, *NE*$^{-/-}$*CatG*$^{-/-}$ *Pr3*$^{-/-}$, *GsdmD*$^{-/-}$ and *Pad4*$^{-/-}$ BMNs 1h30 after *P. a*^{ExoU} infection at an MOI of 2. Scale bar 5µm.

G. Measure of plasma membrane permeabilization over time using SYTOX Green incorporation in WT, *GsdmD*$^{-/-}$ or *Pad4*$^{-/-}$ murine BMNs infected with *P. a*^{ExoU} or *P. a*^{ExoUS142A} in presence or absence of MAFP (20µM). ***p ≤ 0.001, T-test with Bonferroni correction. Values are expressed as mean ± SEM.

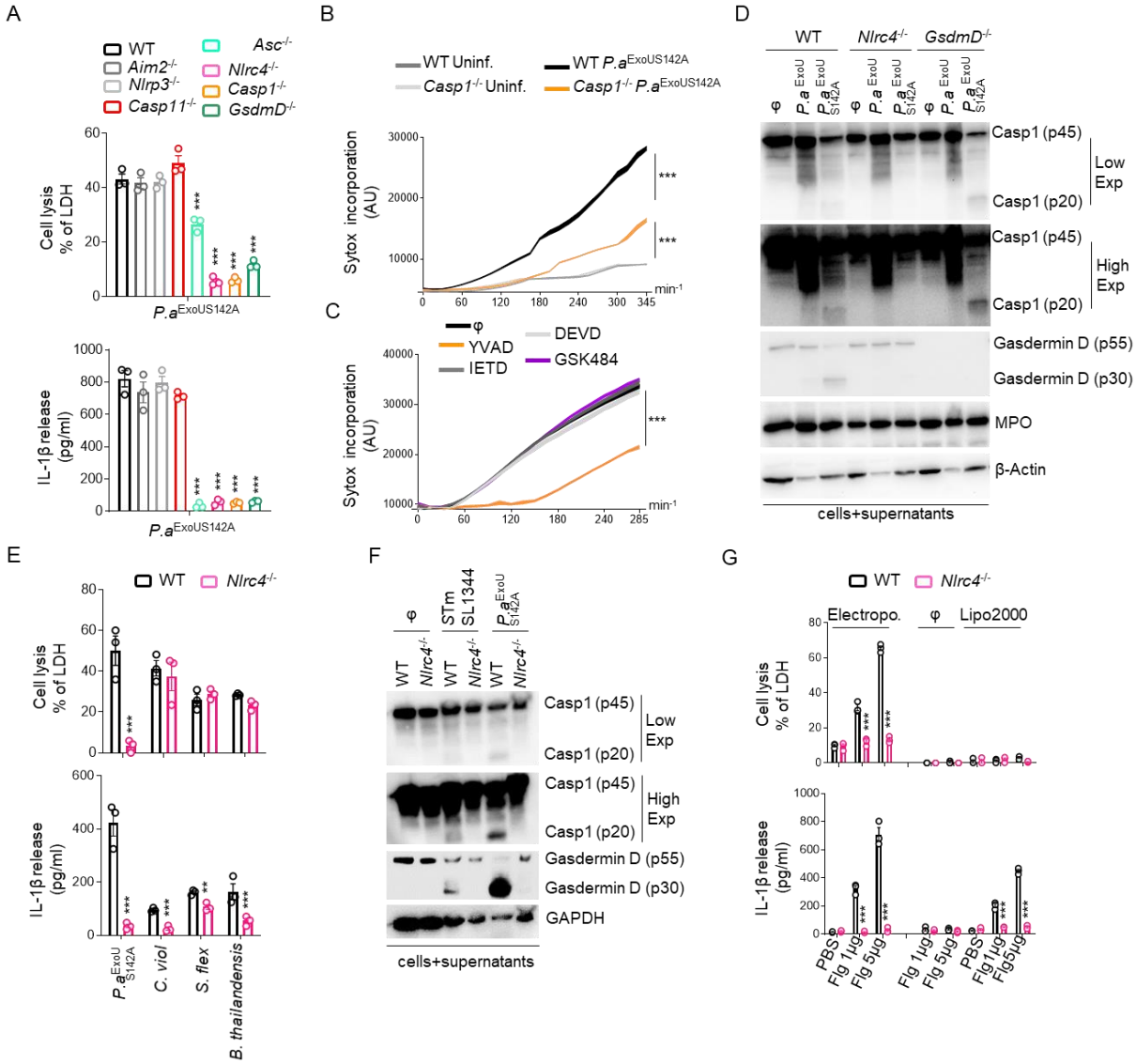

Figure 3. *P. aeruginosa*$^{ExoU-}$ triggers canonical NLRC4 inflammasome-dependent pyroptosis in neutrophils.

Otherwise specified, neutrophils were infected for 3 hours with *P. a*^{ExoU} or *P. a*^{ExoUS142A} at a MOI of 2.

A. Measure of cell lysis (release of LDH) and IL-1β release in WT, *Aim2*$^{-/-}$, *Nlrp3*$^{-/-}$, *Casp11*$^{-/-}$, *Asc*$^{-/-}$, *Nlrc4*$^{-/-}$, *Casp1*$^{-/-}$ and *GsdmD*$^{-/-}$ BMNs infected for 3 hours with *P. a*^{ExoUS142A}. ***p ≤ 0.001, T-test with Bonferroni correction. Values are expressed as mean ± SEM.

B, C. Time course measure of plasma membrane permeabilization using SYTOX Green incorporation in WT or *Casp1*$^{-/-}$ BMNs (**B**) and in human blood neutrophils (**C**) infected *P. a*^{ExoUS142A} in presence or absence of GSK484 (10µM, Pad4 inhibitor), Z-IETD (20µM, Casp8 inhibitor), Z-DEVD (40µM, Casp3/7 inhibitor) or Z-YVAD (40µM,

Casp1 inhibitor). ***p ≤ 0.001, T-test with Bonferroni correction. Values are expressed as mean ± SEM.

D. Immunoblotting of preforms of Caspase-1 (p45) and Gasdermin-D (p55), processed Caspase-1 (p20) and Gasdermin D (p30), Myeloperoxidase (MPO) and β-actin in WT, *Nlrc4*$^{-/-}$ and *GsdmD*$^{-/-}$ BMNs infected for 3 hours with *P. a*^{ExoU} or *P. a*^{ExoUS142A}. Immunoblots show combined lysates and supernatants from one experiment performed three times.

E. Measure of cell lysis (release of LDH) and IL-1β release in WT and *Nlrc4*$^{-/-}$ BMNs infected for 3 hours with *P. a exoU*^{S142A} (MOI 2), *Chromobacter violaceum* (*C. violaceum*, MOI 20), *Shigella flexneri* (*S. flexneri*, MOI 40) or *Burkholderia thailandensis* (*B. thailandensis*, MOI 40). ***p ≤ 0.001, T-test with Bonferroni correction. Values are expressed as mean ± SEM.

F. Immunoblotting of preforms of Caspase-1 (p45) and Gasdermin-D (p55), processed Caspase-1 (p20) and Gasdermin-D (p30) and GAPDH in WT and *Nlrc4*$^{-/-}$ BMNs infected for 3 hours with *P. a*^{ExoUS142A} (MOI2) or *S*. Typhimurium (*S*.Tm, MOI 10). Immunoblots show combined lysates and supernatants from one experiment performed three times.

G. Measure of cell lysis (release of LDH) and IL-1β release in PAM3CSK4-primed WT and *Nlrc4*$^{-/-}$ BMNs transfected with flagellin (NLRC4 activator, 1µg or 5µg) or electroporated with 1µG or 5µg of flagellin for 3 hours. ***p ≤ 0.001, T-test with Bonferroni correction. Values are expressed as mean ± SEM.

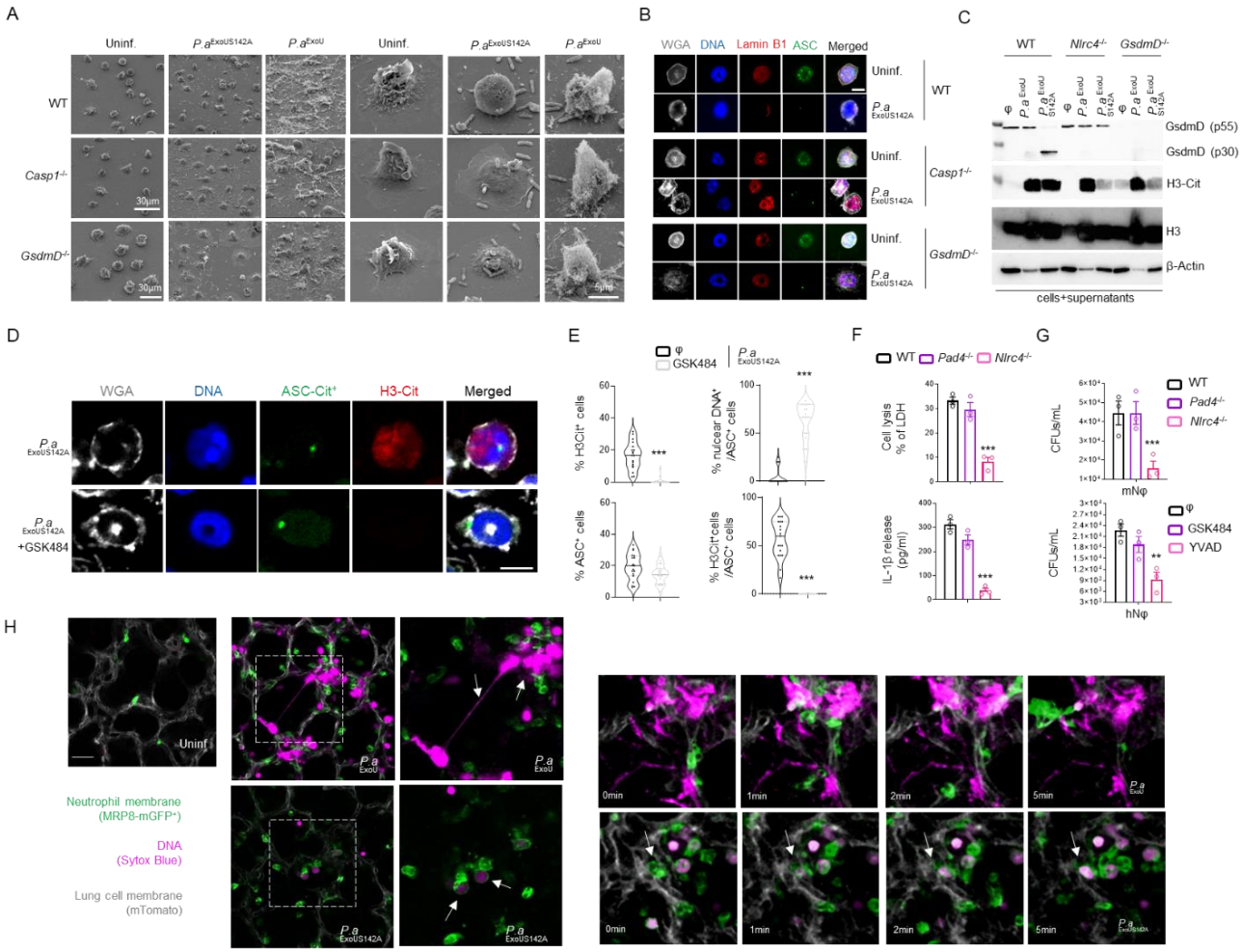

Figure 4. Caspase-1-induced neutrophil pyroptosis generates intracellular but not extracellular decondensed DNA structures in a PAD4-dependent manner

A. Scanning electron microscopy (SEM) observation of pyroptosis in WT, *Casp1*$^{-/-}$ and *GsdmD*$^{-/-}$ BMNs 3 hours after *P. a*^{ExoUS142A} infection at an MOI of 2.

B. Confocal microscopy observations of *P. a*^{ExoUS142A}-infected BMNs for 3 hours harboring ASC complexes, decondensed DNA and nuclear membrane (LaminB1). Nucleus (blue) was stained with Hoescht; LaminB1 is in red (anti LaminB1); ASC is in Green (anti-ASC); plasma membrane is in grey (WGA staining). Scale bar 10µm.

C. Immunoblotting of Citrullinated Histone-3 (H3Cit), preformed and cleaved Gasdermin-D (p55/p30) and β-Actin in WT, *Nlrc4*$^{-/-}$ and *GsdmD*$^{-/-}$ BMNs infected for 3 hours with *P. a*^{ExoU} or *P. a*^{ExoUS142A} at an MOI of 2. Immunoblots show combined lysates and supernatants from one experiment performed three times.

D, E. Confocal microscopy observations (**D**) and quantifications (**E**) of the percentage of cells harboring ASC complexes, H3Cit and nuclear DNA in WT-ASC-Citrine^{+} BMNs infected for 3hours with *P. a*^{ExoUS142A} in presence/absence of the PAD4 inhibitor

GSK484 (10µM). Nucleus (blue) was stained with Hoescht; Histone-3 Citrullination is in red (Anti-H3Cit staining); plasma membrane is in grey (WGA staining). Scale bar 10µm. For quantifications, the percentage of cells with ASC complexes, nuclear DNA or positives for H3Cit (H3-Cit^{+}) was determined by determining the ratios of cells positives for ASC speckles, nuclear DNA or H3Cit. At least 10 fields from n=3 independent experiments were analyzed. Values are expressed as mean ± SEM.

F. Measure of cell lysis (release of LDH) and IL-1β release in WT, *Pad4*$^{-/-}$ and *Nlrc4*$^{-/-}$ BMNs infected for 3 hours with *P. a*$^{\text{ExoUS142A}}$. ***p ≤ 0.001, T-test with Bonferroni correction. NS: Not significant. Values are expressed as mean ± SEM.

G. Microbicidal activity of murine WT, *Nlrc4*$^{-/-}$ and *Pad4*$^{-/-}$ BMNs or human blood neutrophils (3h) after infection with *P. a*$^{\text{ExoUS142A}}$ in presence/absence of GSK484 (10µM, Pad4 inhibitor) or Z-YVAD (40µM, Casp1 inhibitor). ***p ≤ 0.001, T-test with Bonferroni correction. Values are expressed as mean ± SEM.

H. Intravital microscopy visualization of granulocyte death in MRP8-GFP^{+} mice infected with 2.5.10^{5} CFUs of *P. a*$^{\text{ExoU}}$ or *P. a*$^{\text{ExoUS142A}}$ in presence of Sytox Blue for 10 hours. Granulocyte death was observed in infected lungs by the appearance of Sytox blue fluorescence. Pseudo colors represent vessels (gray, mTG); Granulocytes (Blue, MRP8-GFP^{+}); Dead cells (Yellow, Sytox blue). Scale bar: 20µm.

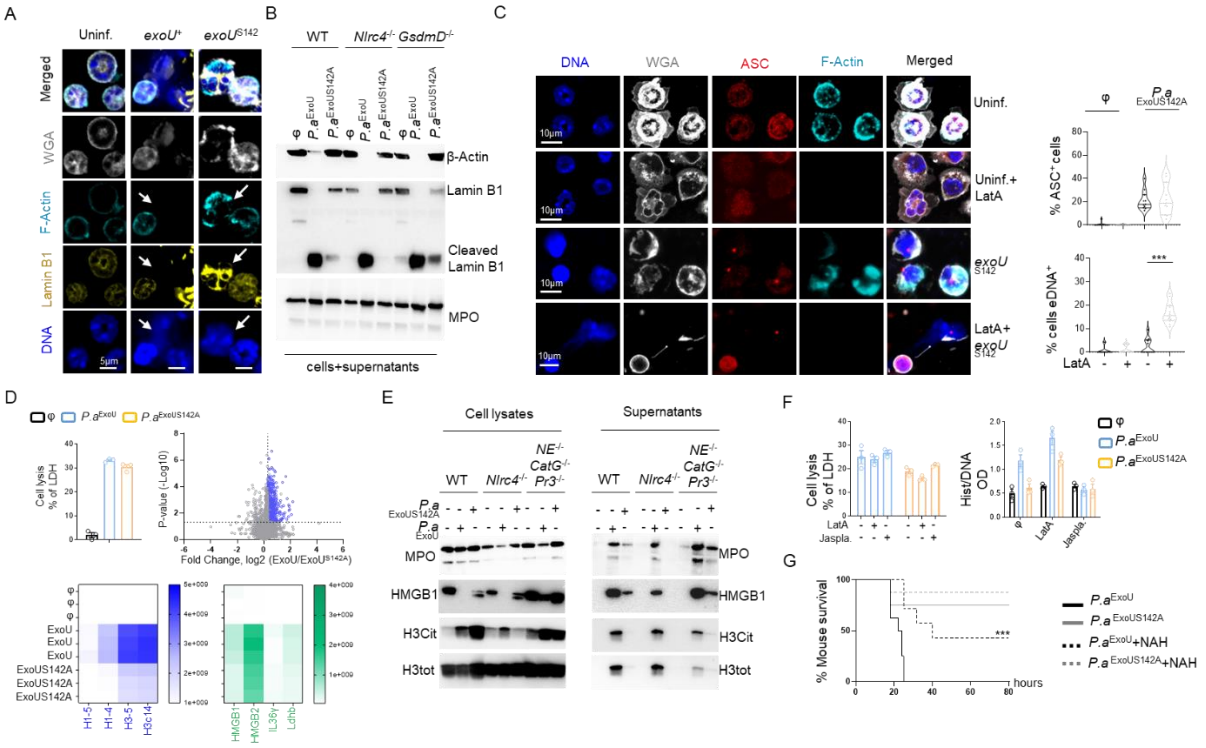

Figure 5. Subcortical actin cytoskeleton limits DNA-associated Histone exposure upon Caspase-1-induced pyroptosis

A. Confocal microscopy observations of the presence or not of subcortical actin (F-Actin) and nuclear envelop (lamin-B1) cytoskeleton integrity in WT BMNs infected for 3hours with *P. a*^{ExoU} or *P. a*^{ExoUS142A}. DNA (blue) was stained with Hoescht; F-Actin is in cyan (phalloidin); Lamin-B1 is in yellow (anti-lamin-B1); plasma membrane is in grey (WGA staining). Scale bar 10µm.

B. Immunoblotting of cytoskeletal components B-Actin, Lamin-B1, Vimentin, γ-Tubulin WT and *Nlrc4*$^{-/-}$ BMNs infected for 3 hours with *P. a*^{ExoU} or *P. a*^{ExoUS142A}. Immunoblots show combined lysates and supernatants from one experiment performed three times.

C. Confocal microscopy observations and quantification determination of the presence or not of NETs in WT-ACS-Citrine BMNs infected for 3hours with *P. a*^{ExoUS142A} in presence or absence of Latrunculin A (2µM, actin depolimerization inducer). DNA (blue) was stained with Hoescht; F-Actin is in cyan (phalloidin); ASC-Citrine is in red; plasma membrane is in grey (WGA staining). Scale bar 10µm. For quantifications, the percentage of cells with ASC positive structures (%ASC specks) or extracellular DNA (eDNA^{+}) was determined by combining the ratios of cells positives for eDNA (outside from plasma membrane) over the total cellular counts from at least 10 fields from n=3 independent experiments. Values are expressed as mean ± SEM.

D. Cell lysis (LDH release), volcano plot and heat map showing released factors by netotic and pyroptotic BMNs infected for 3 hours with *P. a*^{ExoU} (MOI 0.5) or *P. a*^{ExoUS142A} (MOI 2). Vocano plot show the fold enrichment of released factors induced by *P. a*^{ExoU} over *P. a*^{ExoUS142A}. Heat map show the extracellular abundance of selected DAMPs (Blue; Histones/Green; selected DAMPs). Data are as representative of three biological replicates plotted.

E. Immunoblotting observation of the release of Histone 3, Histone-3 Cit, HMGB1, MPO in supernatant or lysates from pyroptotic and NETotic BMNs infected for 3 hours with *P. a*^{ExoU} (MOI 0.5) or *P. a*^{ExoUS142A} (MOI2). Immunoblots show separated lysates and supernatants from one experiment performed three times.

F. Measure of cell lysis (release of LDH) and Histone/DNA complexes release in WT BMNs infected for 3 hours with *P. a*^{ExoU} (MOI 0.5) or *P. a*^{ExoUS142A} (MOI2). ***p ≤ 0.001, T-test with Bonferroni correction. NS: Not significant. Values are expressed as mean ± SEM.

G. Measure of cell lysis (release of LDH) and Histone/DNA complexes release in WT BMNs infected for 3 hours with *P. a*^{ExoU} (MOI 0.5) or *P. a*^{ExoUS142A} (MOI 2) in presence/absence of actin stabilizing agent jasplakinoid (200nM) or with actin depolymerisating molecule Latrunculin A (2µM). ***p ≤ 0.001, T-test with Bonferroni correction. NS: Not significant. Values are expressed as mean ± SEM.

H. Survival of WT mice intranasally infected (n=8 animals per condition) with 5.10^5 CFUs of *P. a*^{ExoU} or *P. a*^{ExoUS142A}. To ensure both BAL and lung access, PBS or NAH were added both via orbital (15mg/kg) and intranasal (5mg/kg) injections 3 and 9 hours after mice infection. Graphs represent one experiment (8 mice/group) out of three independent in vivo experiments. Log-rank Cox-Mantel test was used for survival comparisons. ***p ≤ 0.001.

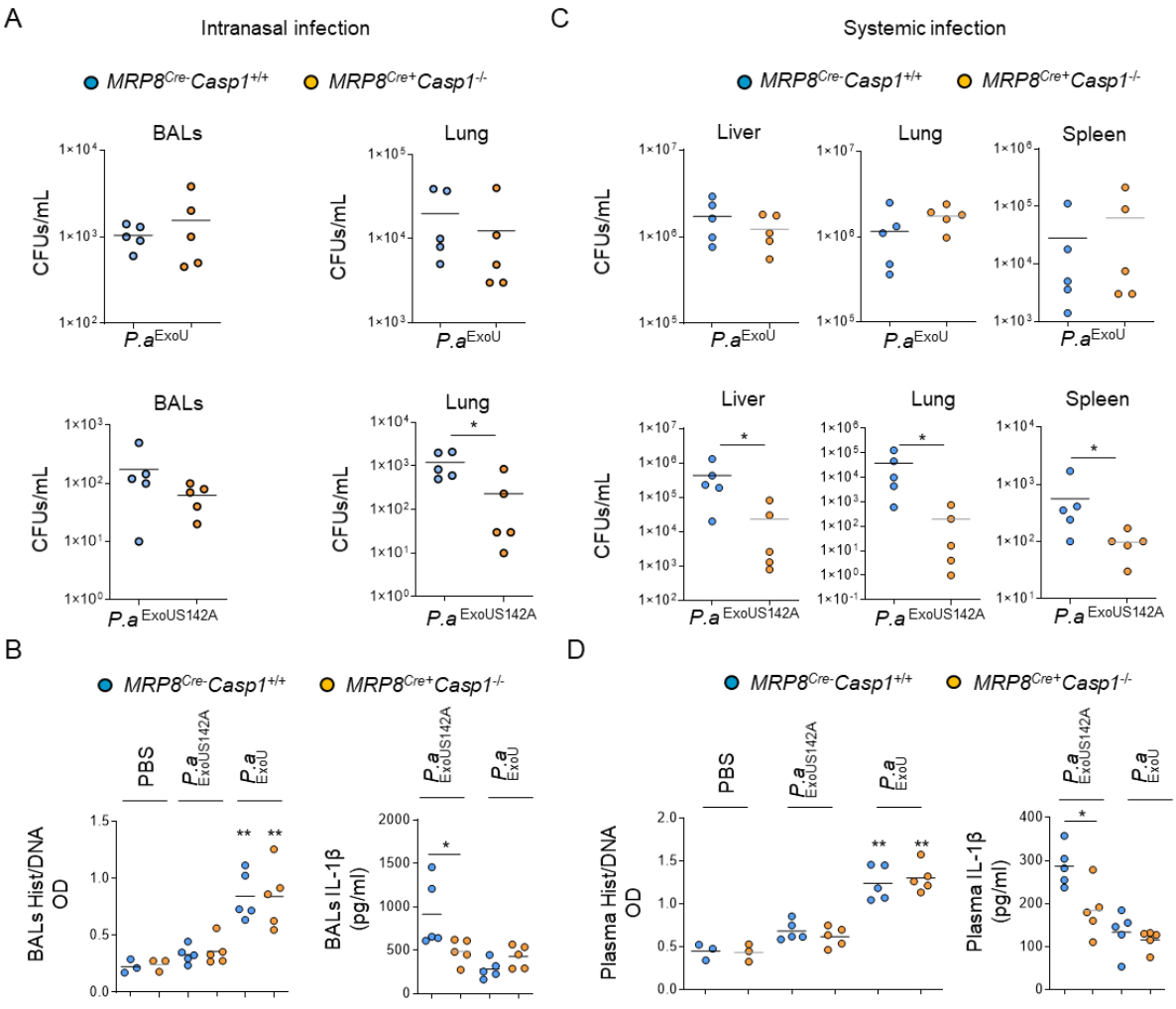

Figure 6. Targeting both neutrophil Caspase-1 and ExoU phospholipase activity synergistically improves *P. aeruginosa* elimination in mice.

A. BAL and lung bacterial loads (colony forming units, CFUs) in MRP8^{Cre-} *Casp1*^{flox} and MRP8^{Cre+}*Casp1*^{flox} mice intranasally infected with 5.10^5 CFUs of *P. a*^{ExoU} or *P. a*^{ExoUS142A} for 24 hours. Graphs represent one experiment (5 mice/group) out of three independent *in vivo* experiments; * p ≤ 0.05, **p ≤ 0.01, Mann-Whitney analysis test.

B. BAL Histone/DNA complexes IL-1β quantifications in MRP8^{Cre-} *Casp1*^{flox} and MRP8^{Cre+}*Casp1*^{flox} mice intranasally infected with 5.10^5 CFUs of *P. a*^{ExoU} or *P. a*^{ExoUS142A} for 10 hours. Graphs represent one experiment (5 mice/group) out of three independent *in vivo* experiments; * p ≤ 0.05, **p ≤ 0.01, Mann-Whitney analysis test.

C. Liver, spleen and lung bacterial loads (CFUs) in MRP8^{Cre-} *Casp1*^{flox} and MRP8^{Cre+}*Casp1*^{flox} mice 24 hours after systemic infection with 1.10^7 CFUs (5 mice/group) of *P. a*^{ExoU} or *P. a*^{ExoUS142A}. Graphs represent one experiment (5 mice/group) out of three independent *in vivo* experiments; * p ≤ 0.05, **p ≤ 0.01, Mann-Whitney analysis test.

D. Determination of plasma Histone/DNA complexes and IL-1β levels in MRP8^{Cre-}*Casp1*^{flox} and MRP8^{Cre+}*Casp1*^{flox} mice at 10 hours after systemic infection with 1.10^{7} CFUs (5 mice/group) of *P. a*^{ExoU} or *P. a*^{ExoUS142A}. Graphs represent one experiment (5 mice/group) out of three independent *in vivo* experiments; * p ≤ 0.05, **p ≤ 0.01, Mann-Whitney analysis test.

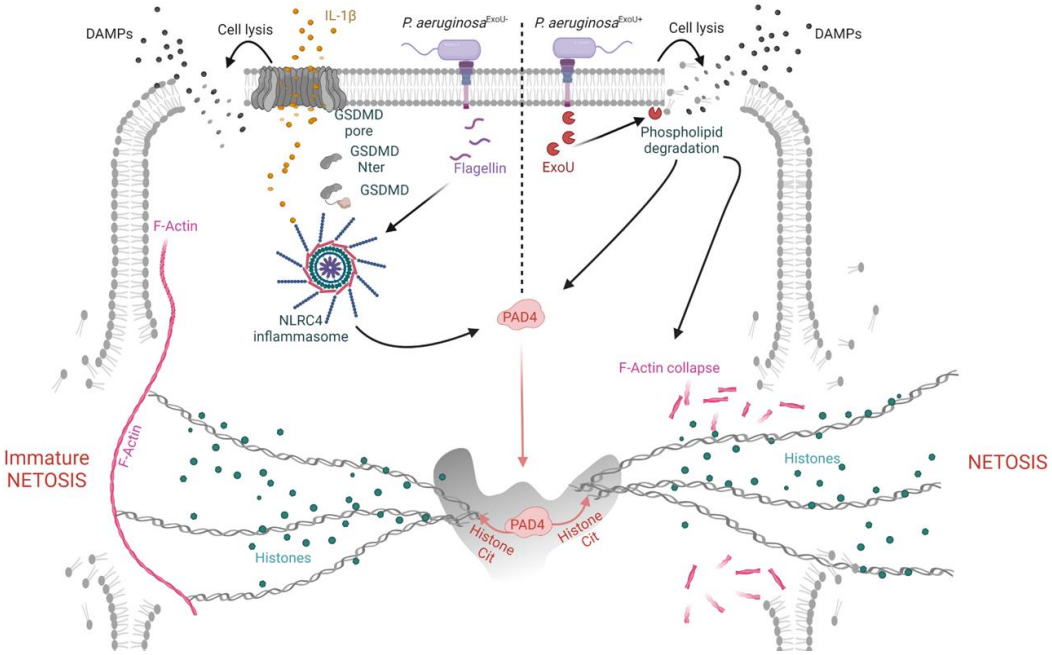

Graphical abstract. *P.aeruginosa*^{ExoU} (right) triggers phospholipid degradation and subsequent neutrophil lysis that associates to NETosis through F-Actin collapse/degradation and PAD4-dependent DNA decondensation. *P.aeruginosa*$^{ExoU-}$ (left) triggers NLRC4-dependent pyroptosis in neutrophils, which leads to PAD4-depndent DNA decondensation but not expulsion due to a still function subcortical F-Actin network. Created with Biorender.com.

STAR Methods

All reagents, concentrations of use and their references are listed in the **Reagent Table**

Mice

Nlrc4$^{-/-}$ (Man et al., 2014b), *Nlrp3*$^{-/-}$ (Martinon et al., 2006), *ASC*$^{-/-}$, *Casp11*$^{-/-}$ (Li et al., 1995; Wang et al., 1998), *Casp1*$^{-/-}$*Casp11*$^{-/-}$ (Li et al., 1995; Wang et al., 1998), *GsdmD*$^{-/-}$, *Aim2*$^{-/-}$, *Pad4*$^{-/-}$, *Gp91phox*$^{-/-}$, *NE*$^{-/-}$*CatG*$^{-/-}$*Pr3*$^{-/-}$ (Yan et al., 2016), *ASC*^{Citrine}, *MRP8*$^{Cre+}$*GFP*$^{+}$ were generated and described in previous studies. Mice were bred at the IPBS (Toulouse, France) and INRAE (Tours Nouzilly, France) animal facilities in agreement to the EU and French directives on animal welfare (Directive 2010/63/EU). Charles Rivers provided WT C57BL/6 mice. Mice experiments are under legal authorizations APAFIS#8521-2017041008135771 and APAFIS#12812-2018031218075551, according to the local, French and European ethic laws.

MRP8^{Cre}*Casp1*^{flox} mice genotyping

Casp1$^{flox/flox}$ mice were crossed to MRP8^{Cre} mice to generate MRP8^{Cre}*Casp1*^{flox}. *Caspase-1* genotyping was performed using Primer Fw: CGAGGGTTGGAGCTCAAGTTGACC and Primer Rv: CACTTTGACTTCTCTAAGGACAG. *Cre* genotyping was performed using Primers Fw: CGCCGTAAATCAATCGATGAGTTGCTTC and Primers Rv: GATGCCGGTGAACGTGCAAAACAGGCTC.

Bacterial cultures

P. aeruginosa strains (PP34, PA14, PA103) and their isogenic mutants were grown overnight in Luria Broth (LB) medium at 37°C with constant agitation. Otherwise specified, all along the study the clinical isolate PP34, referred as *P.a*^{ExoU}, or its isogenic mutants referred as *P.a*^{ExoUS142A}, *P.a*$^{ExoU-}$, *P.a*$^{ExoU-FliC-}$, *P.a*$^{ExsaA-}$ were used. Bacteria were sub-cultured the next day by diluting overnight culture 1:25 and grew until reaching an optical density (OD) O.D.600 of 0.6 – 0.8. Bacterial strains and their mutants are listed in reagent table.

Mice infections

Age and sex-matched animals (5–8 weeks old) per group were infected intravenously (venous-orbital, 50µL with 1.10^7CFUs) or intranasally with 5.10^5 (lethal doses) or $2.5.10^5$ CFUs of various *P. aeruginosa* strains suspended in 25µL of PBS. When specified, intranasal addition of PBS, DNase 1 (4000U/mouse) or N-Acetyl Heparin (NAH) were performed 3 and 9 hours after infections. Specifically, NAH was injected both by intranasal aspiration (25 µL/mouse, 5mg/kg) and by orbital injection (50µL/mouse, 15mg/kg) 3 and 9 hours after infection to ensure both lung and BAL access of NAH. Animals were sacrificed at indicated times after infection and bronchoalveolar fluids (BALFs), blood and lungs were recovered. When specified, bacterial loads (CFU plating), cytokine levels (ELISA) and NET complexes (MPO/DNA, Histone/DNA, ELISA) were evaluated. No randomization or blinding were done.

Intravital microscopy experiments

We relied on the previously published lung intravital microscopy method using an intercoastal thoracic window (Headley et al., 2016; Looney et al., 2011), adapted at the IPBS CNRS-University of Toulouse TRI platform.

MRP8-mTmG mice (8-12 weeks old) were infected intratracheally with 5.10^5 CFUs of *P. aeruginosa* ExoU or ExoU^{S142A} strains resuspended in 50µL of PBS and imaged 6 to 8 hours after infection. 50µL of 50µM solution of Sytox blue (Life Technologies) was injected both intravenously (retroorbital) and intratracheally just before imaging to visualize extracellular DNA.

Next, mice were anesthetized with ketamine and xylazine and secured to a microscope stage. A small tracheal cannula was inserted, sutured and attached to a MiniVent mouse ventilator (Harvard Apparatus). Mice were ventilated with a tidal volume of 10 µl of compressed air (21% O_2) per gram of mouse weight, a respiratory rate of 130-140 breaths per minute, and a positive-end expiratory pressure of 2-3 cm H_2O. Isoflurane was continuously delivered to maintain anesthesia and 300 µl of 0.9% saline solution were i.p. administered in mice every hour for hydration. Mice were placed in the right lateral decubitus position and a small surgical incision was made to expose the rib cage. A second incision was then made into the intercostal space between ribs 4 and 5, through the parietal pleura, to expose the surface of the left lung lobe. A flanged thoracic window with an 8 mm coverslip was inserted between the ribs and secured to the stage using a set of optical posts and a 90° angle post clamp (Thor Labs). Suction was applied to gently immobilize the lung (Dexter Medical). Mice were

placed in 30°C heated box during microscopy acquisition to maintain the body temperature and the 2-photon microscope objective was lowered over the thoracic window. Intravital imaging was performed using a Zeiss 7MP upright multi-photon microscope equipped with a 20×/1.0 objective and a Ti-Sapphire femtosecond laser, Chameleon-Ultra II (Coherent Inc.) tuned to 920 nm. Sytox Blue, GFP and Tomato emission signals were detected thanks to the respective bandpass filters: Blue (SP485), Green (500-550) and Red (565-610). Images were analyzed using Imaris software (Bitplane) and Zen (Zeiss).

Isolation of primary murine neutrophils

Murine Bone marrow cells were isolated from tibias and femurs, and neutrophils were purified by positive selection using Anti-Ly-6G MicroBead Kit (Miltenyi Biotech) according to manufacturer's instructions. This process routinely yielded >95% of neutrophil population as assessed by flow cytometry of $Ly6G^+/CD11b^+$ cells.

Isolation of primary human neutrophils

Whole blood was collected from healthy donors by the "Ecole française du sang" (EFS, Tolouse Purpan, France) in accordance with relevant guidelines. Written, informed consent was obtained from each donor. Neutrophils were then isolated by negative selection using MACSxpress® Whole Blood Human Neutrophil Isolation Kit (Miltenyi Biotech) according to manufacturer's instructions. Following isolations cells were centrifuged 10 min at 300 g and red blood cells were eliminated using Red blood cells (RBC) Lysis Buffer (BioLegend). This procedure gives >95% of neutrophil population as assessed by flow cytometry of CD15+/CD16+ cells. License to use human samples is under legal agreement with the EFS; contract n° 21PLER2017-0035AV02, according to Decret N° 2007-1220 (articles L1243-4, R1243-61).

Cell plating and treatment of Neutrophils

Following isolation, Neutrophils were centrifugated for 10 min at 300 g and pellet was resuspendent in serum free OPTI-MEM medium. Absolute cell number was determined with automated cell counter Olympus R1 with trypan blue cell death exclusion method (typically living cells represent >70% of cell solution) and cell density was adjusted at 10^6 / mL by adding OPTI-MEM culture medium. Neutrophils were then plated in either 96 well plates, 24 well plates or 6 well plates with 100 µL (10^5 cells),

500 µL (5.10^5 cells) or 2 mL (2.10^6 cells) respectively. When indicated cells were primed with Pam_3CSK_4 (100 ng/ml) or LPS (100 ng/ml) for 2 hrs and/or incubated with chemical inhibitors Z-VAD-fmk (20 µM), Y-VAD-fmk (40 µM), GSK484 (10 µM), Latrunculin A (2 µM), Jasplakinolide (200 nM) as indicated in each experimental setting. Neutrophils were infected with various bacterial strains and multiplicity of infections (M.O.I.) as indicated.

Electroporation / transfection of flagellin

Before electroporation/transfection neutrophils were first primed with Pam_3CSK_4 (1 $\mu g.mL^{-1}$) for 2 hrs, and washed with PBS. Recombinant flagellin (FLA-PA, invivoGen) 1 to 5 µg was electroparated into ~2.0×10^6 cells in 20 µL of Tampon R (R buffer) using the Neon transfection system (Life Technologies). Settings were the following: 1720 Voltage, 10 Width, 2 Pulse. After electroporation cells were plated in 6 or 24 well plates and incubated for 3hrs before further experiments. For transfection, 1 to 5 µg of flagellin was mixed with 0.1% v/v Lipofectamine 2000 (Life Technologies) in Optimem medium, incubated for 5 min at room temperature, and transfected into ~2.0×10^6 cells in 6 or 24 well plates. Cells were incubated for 4hrs before further manipulations.

Kinetic analysis of Neutrophil's permeability by SYTOX Green incorporation assay

Cells are plated at density of 1 x 10^5 per well in Black/Clear 96-well Plates (REF) in OPTI-MEM culture medium supplemented with SYTOX-Green dye (100ng/mL) and infected/treated as mentioned in figure legend. Green fluorescence are measured in real-time using Clariostar plate reader equipped with a 37°C cell incubator.

ELISA and plasma membrane lysis tests

Cell death was measured by quantification of the lactate dehydrogenase (LDH) release into the cell supernatant using LDH Cytotoxicity Detection Kit (Takara). Briefly, 100 µL cell supernatant were incubated with 100 µL LDH substrate and incubated for 15 min. The enzymatic reaction was stopped by adding 50 µL of stop solution. Maximal cell death was determined with whole cell lysates from unstimulated cells incubated with 1% Triton X-100. Human and mouse IL-1β secretion was quantified by ELISA kits (Thermo Fisher Scientific) according to the manufacturer's instructions.

991

992 **Quantification of NETs**

993 Histone/DNA complexes in cells supernatant or serum sample were quantified using
994 Cell Death Detection ELISA^{PLUS} according to manufacturer's instructions (roche).
995 MPO/DNA complexes was assessed as describes previously (Lefrançais et al., 2018).
996 Citrullinated Histone H3/DNA complexes quantification assay was build "in house" and
997 performed similarly to standard ELISA procedure (Thermo Fisher Scientific).
998 Specifically we used anti-Citrullinated H3 antibody (1/1000 in PBS) as capture antibody
999 and anti H3 tot-biot (KIT Cell death roche 1/200) as detection antibody.

1000

1001 **Preparation of neutrophil lysates and supernatant for immunoblot**

1002 At the end of the treatment 5 mM of diisopropylfluorophosphate (DFP) cell permeable
1003 serine protease inhibitor was added to cell culture medium. Cell' Supernatant was
1004 collected and clarified from non-adherent cells by centrifugation for 10 min at 300 g.
1005 Cell pellet and adherent cells were lysed in 100 µL of RIPA buffer (150 mM NaCl,
1006 50 mM Tris-HCl, 1% Triton X-100, 0.5% Na-deoxycholate) supplemented with 5 mM
1007 diisopropylfluorophosphate (DFP) in addition to the protease inhibitor cocktail (Roche).
1008 Cell scrapper was used to ensure optimal recovery of cell lysate. Collected cell lysate
1009 was homogenized by pipetting up and down ten times and supplemented with laemli
1010 buffer (1X final) before boiling sample for 10 min at 95°C. Soluble proteins from cell
1011 supernatant fraction were precipitated as described previously (Eren et al., 2020).
1012 Precipitated pellet was then resuspended in 100 µL of RIPA buffer plus laemli
1013 supplemented with 5 mM diisopropylfluorophosphate (DFP) and protease inhibitor
1014 cocktail (Roche) and heat denaturated for 10 min at 95°C. Cell lysate and cell
1015 supernatant fraction were then analysed by immunoblot either individually or in pooled
1016 sample of lysate plus supernatant (equal vol/vol).

1017

1018 **Treatment of Neutrophils for Immunofluorescences**

1019 5.10^5 Cells were plated on 1.5 glass coverslips in 24 well plate and infected/treated as
1020 described above. At the end of the assay, cell supernatant was removed and cells were
1021 fixed with a 4% PFA solution (ref) for 10 min at 37°C. PFA was then removed and cells
1022 were washed 3 times with HBSS. When desired, plasma membrane was stained with
1023 Wheat Germ Agglutinin, Alexa Fluor™ 633 Conjugate (ThermoFisher Scientifique) at
1024 1/100th dilution in HBSS, and incubated for 30 min under 100 rpm orbital shaking

conditions. Then cells were washed with HBSS and processed for further staining. Permeabilization was performed by incubating cells for 10 min in PBS containing 0.1% Triton X-100. To block unspecific binding of the antibodies cells are Incubated in PBS-T (PBS+ 0.1% Tween 20), containing 2% BSA, 22.52 mg/mL glycine in for 30 min. 3 washes with PBS-T was performed between each steps. Primary antibodies staining was performed overnight at 4°C in BSA 2% - Tween 0.1% - PBS (PBS-T) solution. Coverslips were washed three times with PBS-T and incubated with the appropriate fluor-coupled secondary antibodies for 1 hour at room temperature. DNA was counterstained with Hoechst. Cells were then washed three times with PBS and mounted on glass slides using Vectashield (Vectalabs). Coverslips were imaged using confocal Zeiss LSM 710 (INFINITY, Toulouse) or Olympus Spinning disk (Image core Facility, IPBS, Toulouse) using a 63x oil objective. Unless specified, for each experiment, 5-10 fields (~50-250 cells) were manually counted using Image J software.

Scanning Electron Microscopy experiments

For scanning electron microscopy observations, cells were fixed with 2.5% glutaraldehyde in 0.2M cacodylate buffer (pH 7.4). Preparations were then washed three times for 5min in 0.2M cacodylate buffer (pH 7.4) and washed with distilled water. Samples were dehydrated through a graded series (25 to 100%) of ethanol, transferred in acetone and subjected to critical point drying with CO2 in a Leica EM CPD300. Dried specimens were sputter-coated with 3 nm platinum with a Leica EM MED020 evaporator and were examined and photographed with a FEI Quanta FEG250.

ImageStreamX

Cells isolated from peritoneal washes were pelleted by centrifugation (10 min at 300 g). Neutrophils were stained prior to fixation with anti-Ly6G (APC-Vio770, Miltenyi-Biotec Clone: REA526 | Dilution: 1:50) in MACS buffer (PBS-BSA 0,5%-EDTA 2mM) in presence of FC block (1/100) and Hoechst (1 µM). Then, cells were fixed in 4% PFA. Data were acquired on ImageStreamXMKII (Amnis) device (CPTP Imaging and Cytometry core facility) and analyzed using IDEAS software v2.6 (Amnis). The gating strategy used to evaluate inflammasome activation in neutrophils was performed as follow: (i) a gate was set on cells in focus [Cells in Focus] and (ii) a sub-gate was created on single cells [Single Cells]. Then we gated first on (iii) LY6G+ Neutrophils

[LY6G+] and second on (iv) ASC-citrine+ and Hoechst+ cells [Hoechst+/ASC-Citrine+] within LY6G+ population. (v) To distinguish cells with active (ASC-speck) versus inactive inflammasome (Diffuse ASC), we plotted the Intensity with the area of ASC-citrine. This strategy allow to distinguish cells with active inflammasome that were visualized and quantified. (**Fig S3E**).

Mass spectrometry

Tryptic peptides were resuspended in 2% acetonitrile and 0.05% trifluoroacetic acid and analyzed by nano-liquid chromatography (LC) coupled to tandem MS, using an UltiMate 3000 system (NCS-3500RS Nano/Cap System; Thermo Fisher Scientific) coupled to an Orbitrap Q Exactive Plus mass spectrometer (Thermo Fisher Scientific). Around 1µg of each sample was loaded on a C18 precolumn (300 µm inner diameter × 5 mm, Thermo Fisher Scientific) in a solvent made of 2% acetonitrile and 0.05% trifluoroacetic acid, at a flow rate of 20 µl/min. After 5 min of desalting, the precolumn was switched online with the analytical C18 column (75 µm inner diameter × 50 cm, in-house packed with Reprosil C18) equilibrated in 95% solvent A (5% acetonitrile, 0.2% formic acid) and 5% solvent B (80% acetonitrile, 0.2% formic acid). Peptides were eluted using a 5%-50% gradient of solvent B over 105 min at a flow rate of 300 nl/min. The mass spectrometer was operated in data-dependent acquisition mode with the Xcalibur software. MS survey scans were acquired with a resolution of 70,000 and an AGC target of 3e6. The 10 most intense ions were selected for fragmentation by high-energy collision induced dissociation, and the resulting fragments were analyzed at a resolution of 17500, using an AGC target of 1e5 and a maximum fill time of 50ms. Dynamic exclusion was used within 30 s to prevent repetitive selection of the same peptide.

Data processing Raw MS files were processed with the Mascot software (version 2.7.0) for database search and Proline (Bouyssie et al, Bioinformatics 2020) for label-free quantitative analysis. Data were searched against *Mus musculus* entries of the UniProtKB protein database (release UniProtKB/Swiss-Prot+TrEMBL 2020_07, 87954 entries). Carbamidomethylation of cysteines was set as a fixed modification, whereas oxidation of methionine and protein N-terminal acetylation were set as variable modifications. Specificity of trypsin digestion was set for cleavage after K or R, and two missed trypsin cleavage sites were allowed. The mass tolerance was set to 10 ppm for

the precursor and to 20 mmu in tandem MS mode. Minimum peptide length was set to 7 amino acids, and identification results were further validated in Proline by the target decoy approach using a reverse database at both a PSM and protein false-discovery rate of 1%. For label-free relative quantification of the proteins across biological replicates and conditions, cross-assignment of peptide ions peaks was enabled with a match time window of 1 min, after alignment of the runs with a time window of +/- 600s.

Statistical tests used

Statistical analysis was performed with Prism 8.0a (GraphPad Software, Inc.). Otherwise specified, data are reported as mean with SEM. T-test with Bonferroni correction was chosen for comparison of two groups. For in vivo mice experiments and comparisons we used Mann-Whitney tests and mouse survival analysis were performed using log-rank Cox-Mantel test. P values are shown in figures with the following meaning; NS non-significant and Significance is specified as *$p \leq 0.05$; **$p \leq 0.01$, ***$p \leq 0.001$.

Table reagents

1126 Reagents and Tools are available upon request to Etienne.meunier@ipbs.fr or
1127 Remi.planes@gmail.com

REAGENT or RESSOURCE	SOURCE	IDENTIFIER
Antibodies		
Anti- mouse Caspase 1, 1: 1000	AdipoGen	AG20B-0042
Anti-Ly6G APC-Vio770, 1:50	Miltenyi-Biotec	**130-119-126**
Anti- mouse Gasdermin D, 1: 1000	Abcam	AB209845
Anti- mouse IL-1beta, 1: 1000	R&D Systems	AF-401-NA
Anti-MPO , 1: 1000	R&D Systems	AF3667
Anti-ASC, IF 1:100	Novus	NBP1-78-977
Anti-HMGB1, 1: 1000	Genetex	GTX-101277
Anti-HMGB1, 1: 1000	abcam	ab18256
Anti- LaminB1, 1: 1000 Blots, 1:250 IF	abcam	AB229025 [EPR22165-121]
Anti-H3 citrullinated, 1: 1000 Blots, 1:250 IF	abcam	AB5103
Anti-H3, 1: 1000	Cell signalling Techonology	3638S
Anti-H4, 1: 1000	Cell signalling Techonology	2935S
Anti-H2A, 1: 1000	Cell signalling Techonology	2578S
Anti-H1, 1: 1000	Abcam	AB134914 [EPR6536]
Anti-PAD4, 1: 1000	Abcam	AB214810 [EPR20706]
Anti-Neutrophil Elastase, 1: 1000	Abcam	AB68672
Anti-NLRC4 1: 1000	Abcam	ab201792 [EPR19733]
Anti-β-actin 1: 1000	Cell signalling Techonology	4967S
Anti-β-actin 1: 5000	Sigma-Aldrich	A1978
Goat anti-mouse HRP (1/4000)	SouthernBiotech	1034-05
Goat-anti-rabbit IgG (H+L), HRP conjugate (1/4000)	Advansta	R-05072-500
Rabbit anti-Goat IgG (H+L) Secondary Antibody, HRP (1/4000)	Invitrogen	81-1620
Goat anti-rabbit IgG (H&L)Dylight 488 (1/1000)	Immunoreagents	GtxRb-003-D488NHSX
Donkey anti-Rabbit IgG Dylight 550 (1/1000)	Immunoreagents	DkxRb-003-D550NHSX
Goat anti-mouse IgG Dylight 550 (1/1000)	Immunoreagents	GtxMu-003-D550NHSX
Goat anti-mouse IgG Dylight 488 (1/1000)	Immunoreagents	GtxMu-003-D488NHSX
Hoescht	Sigma-Aldrich	H6024
WGA-Alexa 633 (1/100)	Thermo Fisher Scientific	W21404
Alexa Fluor™ 488 Phalloidin	Thermo Fisher Scientific	A12379

RNA, DNA primers/sequences		
MRP8-Cre Fw primers	CGCCGTAAATCAATCGATGAGTTGCTTC	
MRP8-Cre Rv primers	GATGCCGGTGAACGTGCAAAACAGGCTC	
Casp1flox Fw primers	CGAGGGTTGGAGCTCAAGTTGACC	
Casp1flox Rv primers	CACTTTGACTTCTCTAAGGACAG	
Chemicals, peptides and recombinant proteins		
LPS E.Coli K12 (500ng/mL)	Invivogen	tlrl-peklps
FLA-Pa Ultrapure	Invivogen	tlrl-pafla
Pam3CSK4 (200 ng/mL)	Invivogen	tlrl-pm2s-1
DFP (5mM)	Sigma-Aldrich	D0879
Histone from calf thymus	Sigma Aldrich	H9250-100MG
N-Acetylheparin sodium salt	Sigma Aldrich	A8036-25MG
DNase I from bovine pancreas	Sigma Aldrich	Cat. No. 11 284 932 001
GSK484 (10µM)	Cayman Chemical	17488
Latrunculin A (2µM)	Sigma-Aldrich	**428026**
Jasplakinolide (200nM)	Santa Cruz Biotechonology	sc-202191
ZVAD (20µM)	Invivogen	tlrl-vad
Y-VAD (40µM)	Invivogen	inh-yvad
MAFP (20µM)	Sigma	M2939
SYTOX™ Green Nucleic Acid Stain (100ng/mL)	Thermo Fisher Scientific	S7020
SYTOX™ Blue Nucleic Acid Stain (100ng/mL)	Thermo Fisher Scientific	S11348
PFA (4%)	Sigma-Aldrich	1004969011
cOmplete™ Protease Inhibitor Cocktail	Sigma-Aldrich	11697498001
Lipofectamine-2000	Thermo Fisher Scientific	11668019
Triton X-100	Sigma-Aldrich	X100-500ML
Newborn Calf Serum (FCS)	Thermo Fisher Scientific	16010159
DMEM	Gibco	11574486
HEPES	Invitrogen	15630080
Opti-MEM	Gibco	11524456
RPMI without phenol red	Gibco	11564456
HBSS without Calcium, Magnesium or Phenol Red	Gibco	14-175-095
Clarity Max™ Western ECL Substrate	Bio-Rad	1705062
Tris Base Ultrapure	Euromedex	EU1018-A
SDS Ultrapure 4X	Euromedex	1012-A
Acrylamide / Bisacrylamide 37.5/1 30%	Euromedex	EU0088-B
TEMED	Sigma-Aldrich	T9281
PageRuler™ Prestained Protein Ladder	Thermo Fisher Scientific	11822124
Vectashield	Vectorlabs	H-1000-10
MACSxpress Whole Blood Neutrophil Isolation Kit human	Miltenyi Biotech	130-104-434
Anti-Ly-6G MicroBeads UltraPure, mouse	Miltenyi Biotech	130-120-337
Neon™ Transfection System 100 µL Kit	Thermo Fisher Scientific	MPK10096
Critical comercial assays		

LDH Cytotoxicity Detection Kit	Takara	MK401
IL-1 beta Mouse Uncoated ELISA Kit	Thermo Fisher Scientific	88-7013-88
Cell death detection ELISA PLUS	Sigma-Aldrich	11774425001
Bacterial strains		
PP34	Ina Attrée	(Deruelle et al., 2020)
PP34ExoUS142A	Ina Attrée	(Deruelle et al., 2020)
PP34ExoU-	Ina Attrée	(Deruelle et al., 2020)
PA14	J Buyck	
PA14EXOU-	J Buyck	
PA103	J Buyck	
PA103EXOU-	J Buyck	
Softwares		
Prism v.8		
FlowJo v.10		
ImageLab FiJi		
IDEAS software v2.6 (Amnis)		

Supplemental information

Table S1. List of the identified enriched proteins in the supernatants of *P. aeruginosa*^{ExoU}/*P.aeruginosa*^{ExoUS142A}-infected neutrophils (refers to **Figure 3D**).

Movie S1. Intravital microscopy visualization of granulocyte death in MRP8-GFP$^+$ mice infected with 2.5.10^5 CFUs of *P. a*^{ExoU} in presence of Sytox Blue for 10 hours. Granulocyte death was observed in infected lungs by the appearance of Sytox blue fluorescence. Pseudo colors represent vessels (gray, mTG); Granulocytes (Blue, MRP8-GFP$^+$); Dead cells (Yellow, Sytox blue). Scale bar: 20µm.

Movie S2. Intravital microscopy visualization of granulocyte death in MRP8-GFP$^+$ mice infected with 2.5.10^5 CFUs of *P. a*^{ExoU} or *P. a*^{ExoUS142A} in presence of Sytox Blue for 10 hours. Granulocyte death was observed in infected lungs by the appearance of Sytox blue fluorescence. Pseudo colors represent vessels (gray, mTG); Granulocytes (Blue, MRP8-GFP$^+$); Dead cells (Yellow, Sytox blue). Scale bar: 20µm.

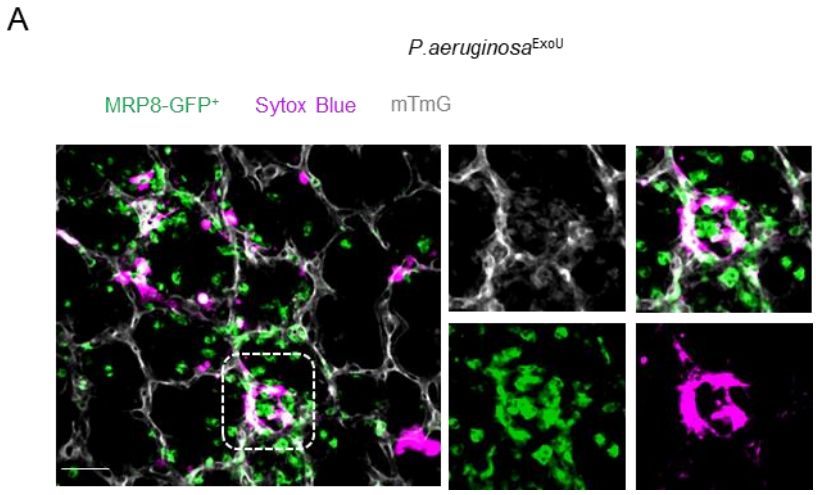

Figure S1. *P. aeruginosa*^{ExoU} triggers NETosi in infected lungs

A. Infected MRP8-GFP$^+$ mice were imaged in presence of Sytox Blue for 10 hours and granulocyte recruitment and death were observed in lungs by the appearance of Green (GFP) and Sytox blue fluorescences. Pseudo colors represent vessels (gray, mTG); Granulocytes (Blue, MRP8-GFP$^+$); Dead cells (Yellow, Sytox blue). Scale bar: 20µm.

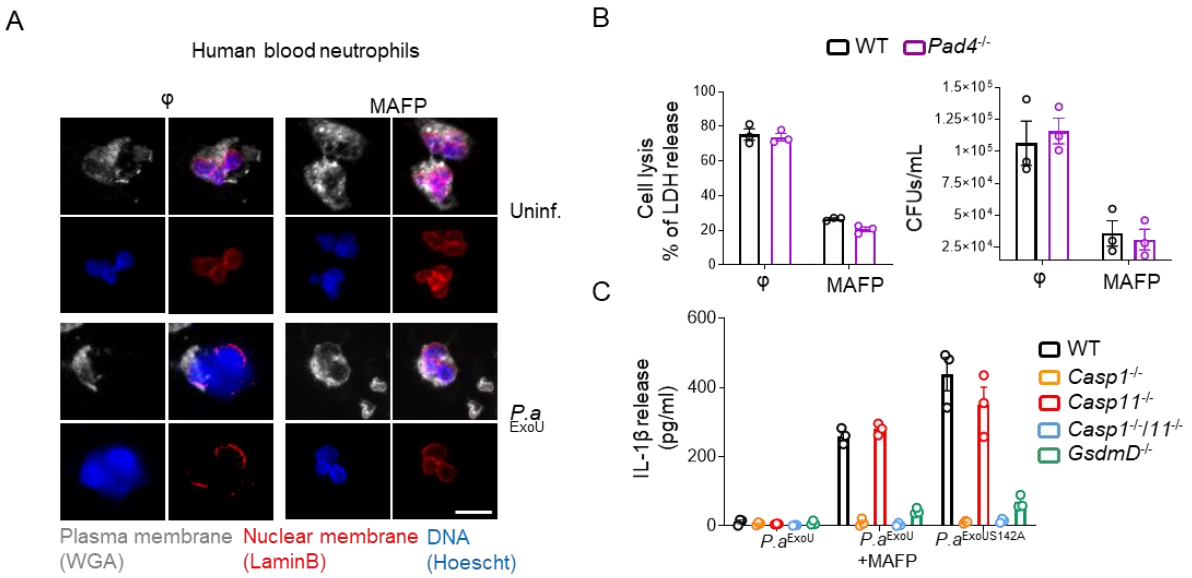

Figure S2. *P. aeruginosa*^{ExoU} promotes PAD4-dependent neutrophil NETosis

A. Confocal microscopy observations of *P. a*^{ExoU}(MOI 2)-infected human blood neutrophils for 1h30 harboring decondensed DNA and destabilized nuclear membrane (LaminB1). When specified MAFP (20µM) was added upon infection. Nucleus (blue) was stained with Hoescht; LaminB1 is in red (anti LaminB1); plasma membrane is in grey (WGA staining). Scale bar 10µm.

B. Measure of cell lysis (release of LDH) and microbicidal activity of WT and *Pad4*$^{-/-}$ murine BMNs infected for 3 hours with *P. a*^{ExoU} (MOI 2). When specified MAFP (20µM) was added upon infection. ***p ≤ 0.001, T-test with Bonferroni correction. NS: Not significant. Values are expressed as mean ± SEM.

C. Measure of IL-1β release in WT, *Casp1*$^{-/-}$, *Casp11*$^{-/-}$, *Casp1*$^{-/-}$*Casp11*$^{-/-}$, *GsdmD*$^{-/-}$ BMNs infected *P. a*^{ExoU} or *P. a*^{ExoUS142A} in presence or absence of MAFP (20µM) for 3 hours. ***p ≤ 0.001, T-test with Bonferroni correction. Values are expressed as mean ± SEM.

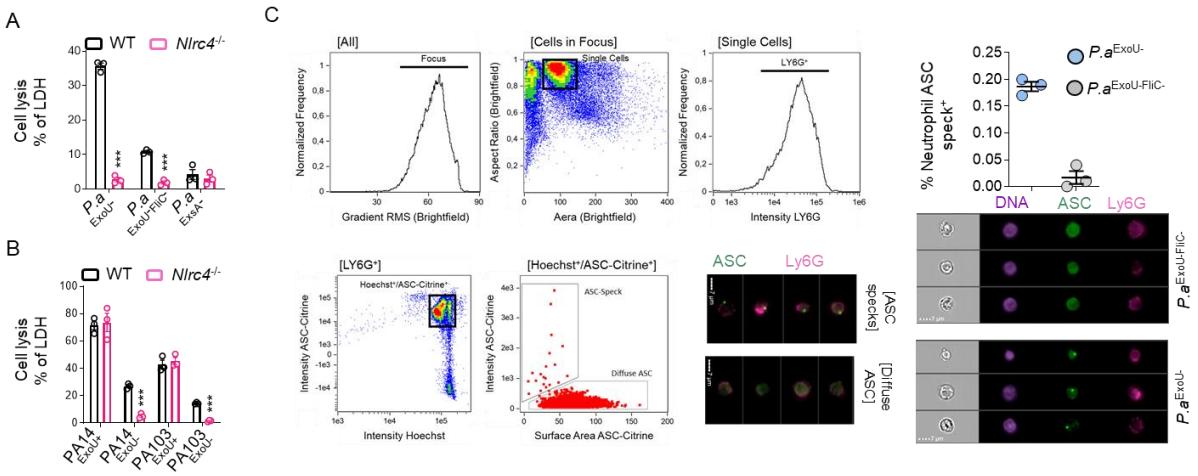

Figure S3. Various *P. aeruginosa* strains elicit NLRC4-dependent pyroptosis of neutrophils

A. Measure of cell lysis (release of LDH) in WT and *Nlrc4*$^{-/-}$ BMNs infected for 3 hours with *P. a*$^{ExoU-}$, *P. a*$^{ExoU-FliC-}$, *P. a*$^{ExsA-}$ at a MOI of 2. ***p ≤ 0.001, T-test with Bonferroni correction. Values are expressed as mean ± SEM.

B. Measure of cell lysis (release of LDH) in WT and *Nlrc4*$^{-/-}$ BMNs infected for 3 hours with PA14 (MOI 5) and PA103 (MOI10) *P. aeruginosa* strains expressing or not ExoU. ***p ≤ 0.001, T-test with Bonferroni correction. Values are expressed as mean ± SEM.

C. Gating strategy and Imagestream experiments for *in vivo* detection of ASC specks in neutrophils in ASC-Citrine mice intranasally infected with 1.10^5 *P. a*$^{ExoU-}$ or *P. a*$^{ExoU-FliC-}$ for 6 hours. The gating strategy used to evaluate inflammasome activation in neutrophils was performed as follow: (i) a gate was set on cells in focus [Cells in Focus] and (ii) a sub-gate was created on single cells [Single Cells]. Then we gated first on (iii) LY6G+ Neutrophils [LY6G+] and second on (iv) ASC-citrine+ and Hoechst+ cells [Hoechst+/ASC-Citrine+] within LY6G+ population. (v) To distinguish cells with active (ASC-speck) versus inactive inflammasome (Diffuse ASC), we plotted the Intensity with the area of ASC-citrine. This strategy allow to distinguish cells with active inflammasome that were visualized and quantified. Values are expressed as mean ± SEM.

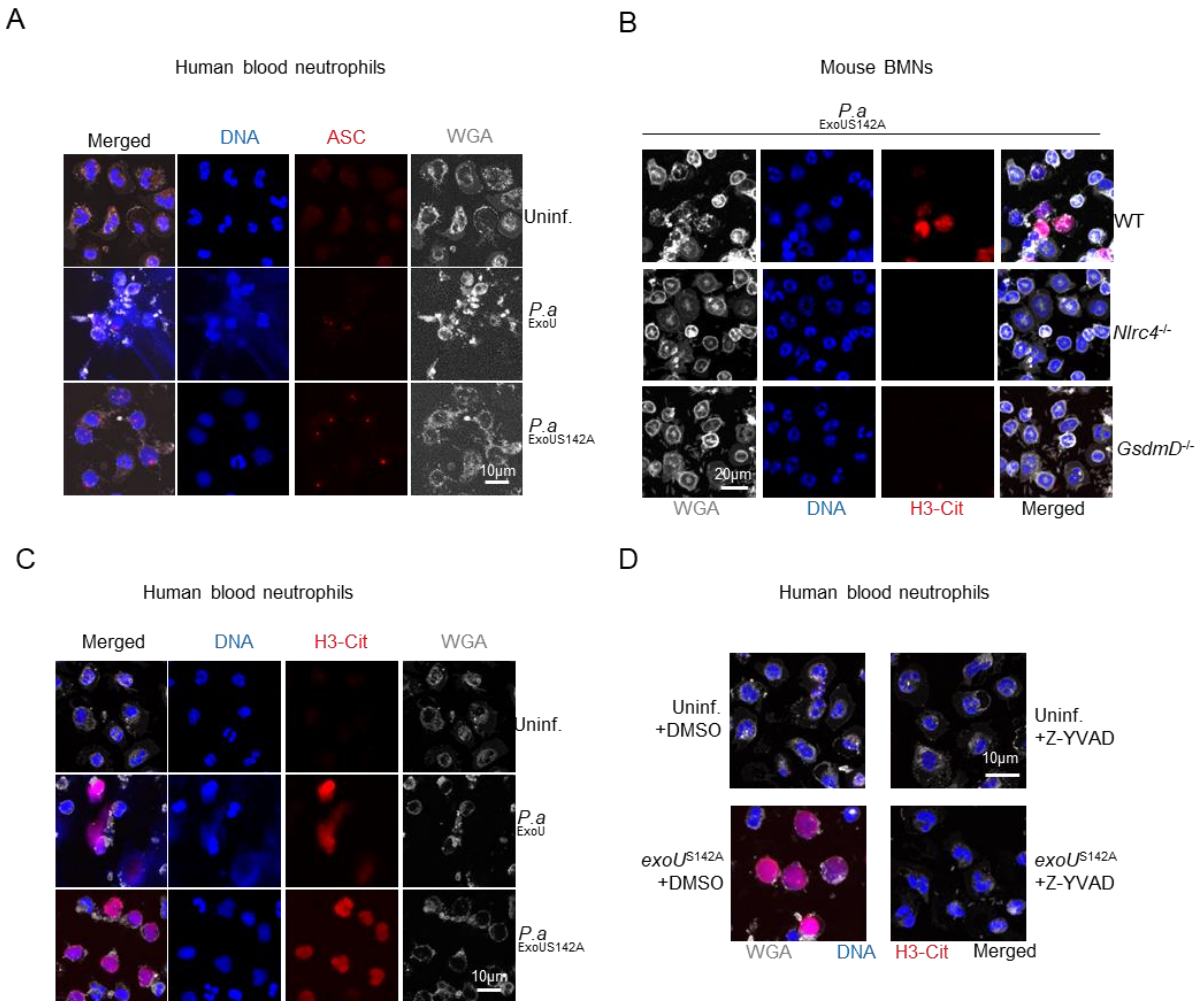

Figure S4. Caspase-1-induced neutrophil pyroptosis does not generate extracellular traps.

A. Confocal microscopy observations of *P. a*^{ExoU}- or *P. a*^{ExoUS142A}-infected human blood neutrophils (MOI 2) for 3 hours harboring ASC complexes and decondensed DNA. Nucleus (blue) was stained with Hoescht; ASC is in red (anti LaminB1); plasma membrane is in grey (WGA staining). Scale bar 10µm.

B, C. Confocal microscopy observations of DNA decondensation and expulsion and Histone-3 Citrullination (H3Cit) in *P. a*^{ExoU}- or *P. a*^{ExoUS142A}-infected (MOI 2) murine BMNs (**B**) or human blood neutrophils (**C**) for 3 hours. Nucleus (blue) was stained with Hoescht; Histone-3 Citrullination is in red (Anti-H3Cit staining); plasma membrane is in grey (WGA staining). Scale bar 10µm.

D. Confocal microscopy observations of *P. a*^{ExoUS142A}-infected human blood neutrophils (MOI 2) for 3 hours harboring H3-Cit and decondensed DNA in presence/absence of the Caspase-1 inhibitor Z-YVAD (40µM). Nucleus (blue) was stained with Hoescht; H3 Cit is in red (anti H3 Cit); plasma membrane is in grey (WGA staining). Scale bar 10µm.

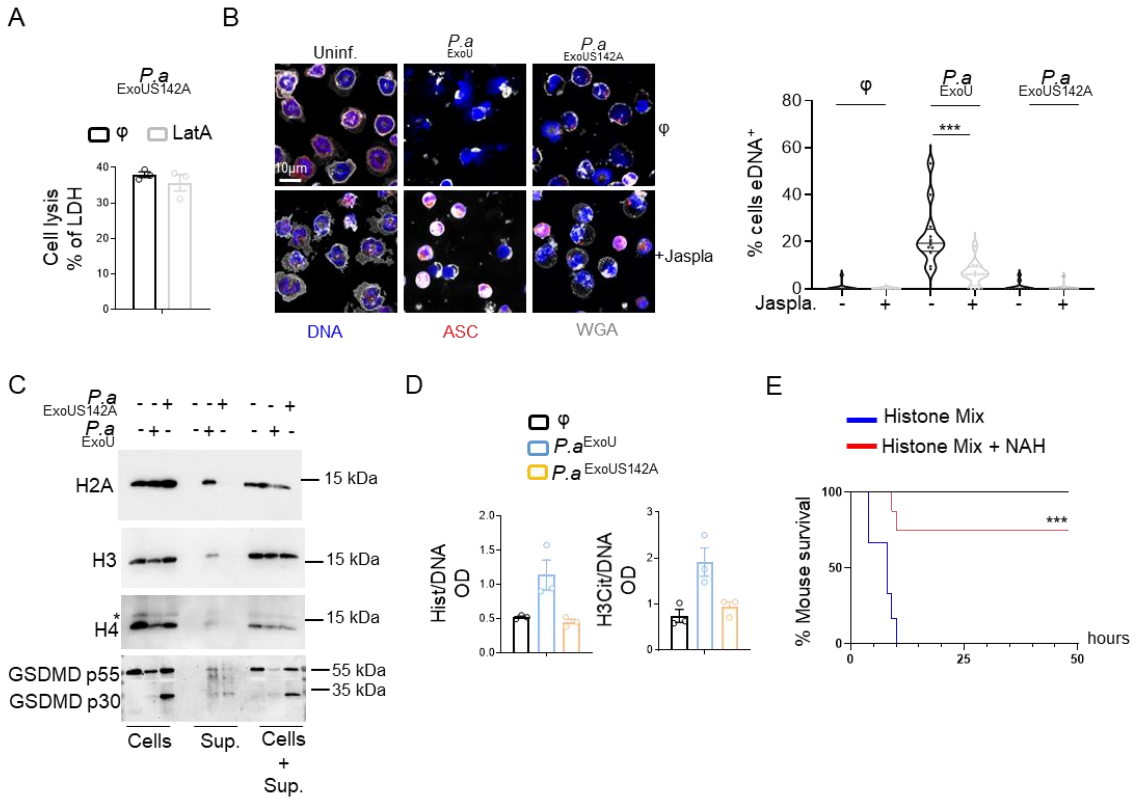

Figure S5. Caspase-1-induced neutrophil pyroptosis restrains the extracellular release of Histones.

A. Measure of cell lysis (release of LDH) in WT BMNs infected for 3 hours with *P. a*^{ExoUS142A} (MOI 2) in presence/absence of actin depolymerisating molecule Latrunculin A (2µM) added 2 hours after infection. T-test with Bonferroni correction. NS: Not significant. Values are expressed as mean ± SEM.

B. Confocal microscopy observations and quantification of the presence or not of NETs in WT-ACS-Citrine BMNs infected for 3hours with *P. a*^{ExoU} or *P. a*^{ExoUS142A} or in presence or absence of Jasplakinolid (200nM, polymerized actin stabilizer). DNA (blue) was stained with Hoescht; ASC-Citrine is in red; plasma membrane is in grey (WGA staining). Scale bar 10µm. For quantifications, the percentage of cells with ASC positive structures (%ASC specks) or extracellular DNA (eDNA^{+}) was determined by combining the ratios of cells positives for eDNA (outside from plasma membrane) over the total cellular counts from at least 10 fields from n=3 independent experiments. Values are expressed as mean ± SEM.

C. Immunoblotting observation of the release of Histones 2A, Histone-3, Histone 4 and GSDMD in supernatant or lysates from pyroptotic and NETotic BMNs infected for 3 hours with *P. a*^{ExoU} (MOI 0.5) or *P. a*^{ExoUS142A} (MOI2). Immunoblots show separated

lysates and supernatants as well as combined samples from one experiment performed three times.

D. Measure of Histone-3/DNA and Histone-3Cit/DNA complexes release in WT BMNs infected for 3 hours with *P. a*^{ExoU} (MOI 0.5) or *P. a*^{ExoUS142A} (MOI 2). ***p ≤ 0.001, T-test with Bonferroni correction. NS: Not significant. Values are expressed as mean ± SEM.

E. Determination of N-Acetyl Heparin (NAH, 20mg/kg)-inhibited toxicity of systemic Histone injection (75mg/kg) in mice. Graphs represent one experiment (8 mice/group) out of three independent in vivo experiments. Log-rank Cox-Mantel test was used for survival comparisons. ***p ≤ 0.001.

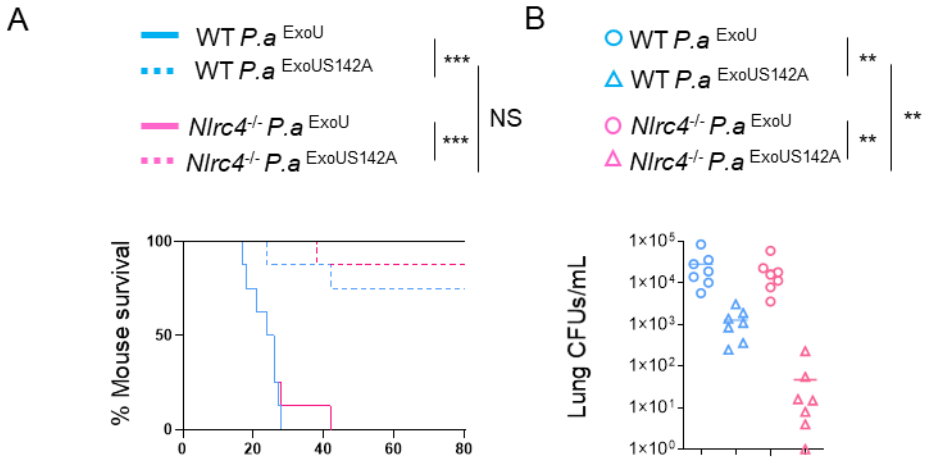

Figure S6. Targeting both the NLRC4 Inflammasome and ExoU synergistically improve *P. aeruginosa* elimination.

A. Survival of WT or *Nlrc4*$^{-/-}$ mice intranasally infected (n=8 animals per condition) with 5.10^5 CFUs of *P. a*^{ExoU} or *P. a*^{ExoUS142A}. Graphs represent one experiment (8 mice/group) out of three independent in vivo experiments. Log-rank Cox-Mantel test was used for survival comparisons. ***p ≤ 0.001.

B. Lung bacterial loads (colony forming units, CFUs) in WT or *Nlrc4*$^{-/-}$ mice intranasally infected with 2.5.10^5 CFUs of *P. a*^{ExoU} or *P. a*^{ExoUS142A} for 24 hours. Graphs represent one experiment (7 mice/group) out of three independent *in vivo* experiments; * p ≤ 0.05, **p ≤ 0.01, Mann-Whitney analysis test.

References

Apel, F., Andreeva, L., Knackstedt, L.S., Streeck, R., Frese, C.K., Goosmann, C., Hopfner, K.-P., and Zychlinsky, A. (2021). The cytosolic DNA sensor cGAS recognizes neutrophil extracellular traps. Sci. Signal. *14*.

Bagayoko, S., Leon Icaza, S., Pinilla, M., Hessel, A., Bordignon, P.-J., Moreau, F., Eren, E., Boyancé, A., Naser, E., Lefèvre, L., et al. (2021). Phospholipid peroxidation fuels ExoU phospholipase-dependent cell necrosis 1 and supports Pseudomonas aeruginosa-driven pathology 2. BioRxiv 2021.02.17.431580.

Biron, B.M., Chung, C.-S., Chen, Y., Wilson, Z., Fallon, E.A., Reichner, J.S., and Ayala, A. (2018). PAD4 Deficiency Leads to Decreased Organ Dysfunction and Improved Survival in a Dual Insult Model of Hemorrhagic Shock and Sepsis. J. Immunol. *200*, ji1700639.

Bjanes, E., Sillas, R.G., Matsuda, R., Demarco, B., Fettrelet, T., Delaney, A.A., Rodriguez Lopez, E.M., Grubaugh, D., Wynosky-Dolfi, M.A., Philip, N.H., et al. (2021). The Card19 locus of murine chromosome 13 regulates terminal cell lysis downstream of caspase activation and Gasdermin-D cleavage Card19 locus regulates caspase-dependent cell lysis. BioRxiv 2021.03.19.436207.

Brinkmann, V., Reichard, U., Goosmann, C., Fauler, B., Uhlemann, Y., Weiss, D.S., Weinrauch, Y., and Zychlinsky, A. (2004). Neutrophil Extracellular Traps Kill Bacteria. Science (80-.). *303*, 1532–1535.

Chen, K.W., Groß, C.J., Sotomayor, F.V., Stacey, K.J., Tschopp, J., Sweet, M.J., and Schroder, K. (2014). The Neutrophil NLRC4 Inflammasome Selectively Promotes IL-1β Maturation without Pyroptosis during Acute Salmonella Challenge. Cell Rep. *8*, 570–582.

Chen, K.W., Monteleone, M., Boucher, D., Sollberger, G., Ramnath, D., Condon, N.D., von Pein, J.B., Broz, P., Sweet, M.J., and Schroder, K. (2018). Noncanonical inflammasome signaling elicits gasdermin D–dependent neutrophil extracellular traps. Sci. Immunol. *3*, 6676.

Chen, K.W., Demarco, B., Heilig, R., Ramos, S.P., Grayczyk, J.P., Assenmacher, C.-A., Radaelli, E., Joannas, L.D., Henao-Mejia, J., Brodsky, I.E., et al. (2021a). RIPK1 activates distinct gasdermins in macrophages and neutrophils upon pathogen blockade of innate immune signalling. BioRxiv 2021.01.20.427379.

Chen, W., Zhao, J., Mu, D., Wang, Z., Liu, Q., Zhang, Y., and Yang, D. (2021b).

Pyroptosis Mediates Neutrophil Extracellular Trap Formation during Bacterial Infection in Zebrafish. J. Immunol. ji2001335.

Cohen, T.S., and Prince, A.S. (2013). Activation of inflammasome signaling mediates pathology of acute P. aeruginosa pneumonia. J. Clin. Invest. *123*, 1630–1637.

D'Cruz, A.A., Speir, M., Bliss-Moreau, M., Dietrich, S., Wang, S., Chen, A.A., Gavillet, M., Al-Obeidi, A., Lawlor, K.E., Vince, J.E., et al. (2018). The pseudokinase MLKL activates PAD4-dependent NET formation in necroptotic neutrophils. Sci. Signal. *11*, 1716.

Demarco, B., Grayczyk, J.P., Bjanes, E., Roy, D. Le, Tonnus, W., Assenmacher, C.A., Radaelli, E., Fettrelet, T., Mack, V., Linkermann, A., et al. (2020). Caspase-8-dependent gasdermin D cleavage promotes antimicrobial defense but confers susceptibility to TNF-induced lethality. Sci. Adv. *6*, 3465–3483.

Deruelle, V., Bouillot, S., Job, V., Taillebourg, E., Fauvarque, M.-O., Attrée, I., and Huber, P. (2020). The bacterial toxin ExoU requires a host trafficking chaperone for transportation and to induce necrosis. BioRxiv 2020.11.04.367706.

Diaz, M.H., and Hauser, A.R. (2010). Pseudomonas aeruginosa cytotoxin ExoU is injected into phagocytic cells during acute pneumonia. Infect. Immun. *78*, 1447–1456.

Eren, E., Planès, R., Bagayoko, S., Bordignon, P., Chaoui, K., Hessel, A., Santoni, K., Pinilla, M., Lagrange, B., Burlet-Schiltz, O., et al. (2020). Irgm2 and Gate-16 cooperatively dampen Gram-negative bacteria-induced caspase-11 response. EMBO Rep. *21*, e50829.

Evavold, C.L., Ruan, J., Tan, Y., Xia, S., Wu, H., and Kagan, J.C. (2018). The Pore-Forming Protein Gasdermin D Regulates Interleukin-1 Secretion from Living Macrophages. Immunity *48*, 35–44.e6.

Evavold, C.L., Hafner-Bratkovič, I., and Kagan, J.C. (2020). Downstream of gasdermin D cleavage, a Ragulator-Rag-mTORC1 pathway promotes pore formation and pyroptosis. BioRxiv 2020.11.02.362517.

Faure, E., Mear, J.-B., Faure, K., Normand, S., Couturier-Maillard, A., Grandjean, T., Balloy, V., Ryffel, B., Dessein, R., Chignard, M., et al. (2014). *Pseudomonas aeruginosa* Type-3 Secretion System Dampens Host Defense by Exploiting the NLRC4-coupled Inflammasome. Am. J. Respir. Crit. Care Med. *189*, 799–811.

Fuchs, T.A., Brill, A., Duerschmied, D., Schatzberg, D., Monestier, M., Myers, D.D., Wrobleski, S.K., Wakefield, T.W., Hartwig, J.H., and Wagner, D.D. (2010). Extracellular DNA traps promote thrombosis. Proc. Natl. Acad. Sci. U. S. A. *107*,

15880–15885.

Galluzzi, L., Vitale, I., Aaronson, S.A., Abrams, J.M., Adam, D., Agostinis, P., Alnemri, E.S., Altucci, L., Amelio, I., Andrews, D.W., et al. (2018). Molecular mechanisms of cell death: Recommendations of the Nomenclature Committee on Cell Death 2018. Cell Death Differ. *25*, 486–541.

Van Gorp, H., Saavedra, P.H.V., De Vasconcelos, N.M., Van Opdenbosch, N., Walle, L. Vande, Matusiak, M., Prencipe, G., Insalaco, A., Van Hauwermeiren, F., Demon, D., et al. (2016). Familial Mediterranean fever mutations lift the obligatory requirement for microtubules in Pyrin inflammasome activation. Proc. Natl. Acad. Sci. U. S. A. *113*, 14384–14389.

Hauser, A.R., and Engel, J.N. (1999). Pseudomonas aeruginosa induces type-III-secretion-mediated apoptosis of macrophages and epithelial cells. Infect. Immun. *67*, 5530–5537.

Headley, M.B., Bins, A., Nip, A., Roberts, E.W., Looney, M.R., Gerard, A., and Krummel, M.F. (2016). Visualization of immediate immune responses to pioneer metastatic cells in the lung. Nature *531*, 513–517.

Heilig, R., Dick, M.S., Sborgi, L., Meunier, E., Hiller, S., and Broz, P. (2018). The Gasdermin-D pore acts as a conduit for IL-1β secretion in mice. Eur. J. Immunol. *48*, 584–592.

Henry, C.M., Sullivan, G.P., Clancy, D.M., Afonina, I.S., Kulms, D., and Martin, S.J. (2016). Neutrophil-Derived Proteases Escalate Inflammation through Activation of IL-36 Family Cytokines. Cell Rep. *14*, 708–722.

Howell, H.A., Logan, L.K., and Hauser, A.R. (2013). Type III secretion of ExoU is critical during early Pseudomonas aeruginosa Pneumonia. MBio *4*.

Kahlenberg, J.M., Carmona-Rivera, C., Smith, C.K., and Kaplan, M.J. (2013). Neutrophil Extracellular Trap–Associated Protein Activation of the NLRP3 Inflammasome Is Enhanced in Lupus Macrophages. J. Immunol. *190*, 1217–1226.

Karmakar, M., Minns, M., Greenberg, E.N., Diaz-Aponte, J., Pestonjamasp, K., Johnson, J.L., Rathkey, J.K., Abbott, D.W., Wang, K., Shao, F., et al. (2020). N-GSDMD trafficking to neutrophil organelles facilitates IL-1β release independently of plasma membrane pores and pyroptosis. Nat. Commun. *11*.

Kayagaki, N., Kornfeld, O.S., Lee, B.L., Stowe, I.B., O'Rourke, K., Li, Q., Sandoval, W., Yan, D., Kang, J., Xu, M., et al. (2021). NINJ1 mediates plasma membrane rupture during lytic cell death. Nature *591*, 131–136.

Kenny, E.F., Herzig, A., Krüger, R., Muth, A., Mondal, S., Thompson, P.R., Brinkmann, V., von Bernuth, H., and Zychlinsky, A. (2017). Diverse stimuli engage different neutrophil extracellular trap pathways. Elife *6*.

Knackstedt, S.L., Georgiadou, A., Apel, F., Abu-Abed, U., Moxon, C.A., Cunnington, A.J., Raupach, B., Cunningham, D., Langhorne, J., Krüger, R., et al. (2019). Neutrophil extracellular traps drive inflammatory pathogenesis in malaria. Sci. Immunol. *4*, 336.

Knight, J.S., Shelef, M.A., Radic, M., Leppkes, M., Gößwein, S., Lindemann, A., Mahajan, A., Maueröder, C., Martini, E., Patankar, J., et al. (2019). Citrullination Licenses Calpain to Decondense Nuclei in Neutrophil Extracellular Trap Formation. Front. Immunol. | Www.Frontiersin.Org *10*, 2481.

Kovacs, S.B., Oh, C., Maltez, V.I., McGlaughon, B.D., Verma, A., Miao, E.A., and Aachoui, Y. (2020). Neutrophil Caspase-11 Is Essential to Defend against a Cytosol-Invasive Bacterium. Cell Rep. *32*.

Kumar, S.V.R., Kulkarni, O.P., Mulay, S.R., Darisipudi, M.N., Romoli, S., Thomasova, D., Scherbaum, C.R., Hohenstein, B., Hugo, C., Müller, S., et al. (2015). Neutrophil extracellular trap-related extracellular histones cause vascular necrosis in severe GN. J. Am. Soc. Nephrol. *26*, 2399–2413.

Kumari, P., Russo, A.J., Wright, S.S., Muthupalani, S., Correspondence, V.A.R., and Rathinam, V.A. (2021). Hierarchical cell-type-specific functions of caspase-11 in LPS shock and antibacterial host defense.

Lefrançais, E., Mallavia, B., Zhuo, H., Calfee, C.S., and Looney, M.R. (2018). Maladaptive role of neutrophil extracellular traps in pathogen-induced lung injury. JCI Insight *3*.

Li, P., Allen, H., Banerjee, S., Franklin, S., Herzog, L., Johnston, C., McDowell, J., Paskind, M., Rodman, L., Salfeld, J., et al. (1995). Mice deficient in IL-1β-converting enzyme are defective in production of mature IL-1β and resistant to endotoxic shock. Cell *80*, 401–411.

Li, P., Li, M., Lindberg, M.R., Kennett, M.J., Xiong, N., and Wang, Y. (2010). PAD4 is essential for antibacterial innate immunity mediated by neutrophil extracellular traps. J. Exp. Med. *207*, 1853–1862.

Li, Y., Li, M., Weigel, B., Mall, M., Werth, V.P., and Liu, M. (2020). Nuclear envelope rupture and NET formation is driven by PKCα-mediated lamin B disassembly. EMBO Rep. *21*, e48779.

Looney, M.R., Thornton, E.E., Sen, D., Lamm, W.J., Glenny, R.W., and Krummel, M.F.

(2011). Stabilized imaging of immune surveillance in the mouse lung. Nat. Methods *8*, 91–96.

Maltez, V.I., Tubbs, A.L., Cook, K.D., Aachoui, Y., Falcone, E.L., Holland, S.M., Whitmire, J.K., and Miao, E.A. (2015). Inflammasomes Coordinate Pyroptosis and Natural Killer Cell Cytotoxicity to Clear Infection by a Ubiquitous Environmental Bacterium. Immunity *43*, 987–997.

Man, S.M., Ekpenyong, A., Tourlomousis, P., Achouri, S., Cammarota, E., Hughes, K., Rizzo, A., Ng, G., Wright, J.A., Cicuta, P., et al. (2014a). Actin polymerization as a key innate immune effector mechanism to control Salmonella infection. Proc. Natl. Acad. Sci. U. S. A. *111*, 17588–17593.

Man, S.M., Hopkins, L.J., Nugent, E., Cox, S., Glück, I.M., Tourlomousis, P., Wright, J.A., Cicuta, P., Monie, T.P., and Bryant, C.E. (2014b). Inflammasome activation causes dual recruitment of NLRC4 and NLRP3 to the same macromolecular complex. Proc. Natl. Acad. Sci. U. S. A. *111*, 7403–7408.

Martinod, K., Fuchs, T.A., Zitomersky, N.L., Wong, S.L., Demers, M., Gallant, M., Wang, Y., and Wagner, D.D. (2015). PAD4-deficiency does not affect bacteremia in polymicrobial sepsis and ameliorates endotoxemic shock. Blood *125*, 1948–1956.

Martinon, F., Pétrilli, V., Mayor, A., Tardivel, A., and Tschopp, J. (2006). Gout-associated uric acid crystals activate the NALP3 inflammasome. Nature *440*, 237–241.

Metzler, K.D., Goosmann, C., Lubojemska, A., Zychlinsky, A., and Papayannopoulos, V. (2014). Myeloperoxidase-containing complex regulates neutrophil elastase release and actin dynamics during NETosis. Cell Rep. *8*, 883–896.

Neubert, E., Meyer, D., Rocca, F., Günay, G., Kwaczala-Tessmann, A., Grandke, J., Senger-Sander, S., Geisler, C., Egner, A., Schön, M.P., et al. (2018). Chromatin swelling drives neutrophil extracellular trap release. Nat. Commun. *9*, 1–13.

Nichols, R.D., Von Moltke, J., and Vance, R.E. (2017). NAIP/NLRC4 inflammasome activation in MRP8+ cells is sufficient to cause systemic inflammatory disease. Nat. Commun. *8*, 1–12.

Ozer, E.A., Nnah, E., DIdelot, X., Whitaker, R.J., Hauser, A.R., and Ochman, H. (2019). The Population Structure of Pseudomonas aeruginosa Is Characterized by Genetic Isolation of exoU+ and exoS+ Lineages. Genome Biol. Evol. *11*, 1780–1796.

Papayannopoulos, V., Metzler, K.D., Hakkim, A., and Zychlinsky, A. (2010). Neutrophil elastase and myeloperoxidase regulate the formation of neutrophil extracellular traps. J. Cell Biol. *191*, 677–691.

1440 Phillips, R.M., Six, D.A., Dennis, E.A., and Ghosh, P. (2003). In Vivo Phospholipase
1441 Activity of the Pseudomonas aeruginosa Cytotoxin ExoU and Protection of Mammalian
1442 Cells with Phospholipase A2 Inhibitors. J. Biol. Chem. *278*, 41326–41332.
1443 Phulphagar, K., Kühn, L.I., Ebner, S., Frauenstein, A., Swietlik, J.J., Rieckmann, J.,
1444 and Meissner, F. (2021). Proteomics reveals distinct mechanisms regulating the
1445 release of cytokines and alarmins during pyroptosis. Cell Rep. *34*, 108826.
1446 Rühl, S., Shkarina, K., Demarco, B., Heilig, R., Santos, J.C., and Broz, P. (2018).
1447 ESCRT-dependent membrane repair negatively regulates pyroptosis downstream of
1448 GSDMD activation. Science (80-.). *362*, 956–960.
1449 Ryu, J.C., Kim, M.J., Kwon, Y., Oh, J.H., Yoon, S.S., Shin, S.J., Yoon, J.H., and Ryu,
1450 J.H. (2017). Neutrophil pyroptosis mediates pathology of P. aeruginosa lung infection
1451 in the absence of the NADPH oxidase NOX2. Mucosal Immunol. *10*, 757–774.
1452 Sato, H., Frank, D.W., Hillard, C.J., Feix, J.B., Pankhaniya, R.R., Moriyama, K., Finck-
1453 Barbançon, V., Buchaklian, A., Lei, M., Long, R.M., et al. (2003). The mechanism of
1454 action of the Pseudomonas aeruginosa-encoded type III cytotoxin, ExoU. EMBO J. *22*,
1455 2959–2969.
1456 Silvestre-Roig, C., Braster, Q., Wichapong, K., Lee, E.Y., Teulon, J.M., Berrebeh, N.,
1457 Winter, J., Adrover, J.M., Santos, G.S., Froese, A., et al. (2019). Externalized histone
1458 H4 orchestrates chronic inflammation by inducing lytic cell death. Nature *569*, 236–
1459 240.
1460 Sollberger, G., Choidas, A., Burn, G.L., Habenberger, P., Lucrezia, R. Di, Kordes, S.,
1461 Menninger, S., Eickhoff, J., Nussbaumer, P., Klebl, B., et al. (2018). Gasdermin D plays
1462 a vital role in the generation of neutrophil extracellular traps. Sci. Immunol. *3*.
1463 Sutterwala, F.S., Mijares, L.A., Li, L., Ogura, Y., Kazmierczak, B.I., and Flavell, R.A.
1464 (2007). Immune recognition of Pseudomonas aeruginosa mediated by the
1465 IPAF/NLRC4 inflammasome. J. Exp. Med. *204*, 3235–3245.
1466 Thiam, H.R., Wong, S.L., Wagner, D.D., and Waterman, C.M. (2020). Cellular
1467 Mechanisms of NETosis. Annu. Rev. Cell Dev. Biol. *36*, 191–218.
1468 Thiama, H.R., Wong, S.L., Qiu, R., Kittisopikul, M., Vahabikashi, A., Goldman, A.E.,
1469 Goldman, R.D., Wagner, D.D., and Waterman, C.M. (2020). NETosis proceeds by
1470 cytoskeleton and endomembrane disassembly and PAD4-mediated chromatin
1471 decondensation and nuclear envelope rupture. Proc. Natl. Acad. Sci. U. S. A. *117*,
1472 7326–7337.
1473 Tsuchiya, K., Hosojima, S., Hara, H., Kushiyama, H., Mahib, M.R., Kinoshita, T., and

Suda, T. (2021). Gasdermin D mediates the maturation and release of IL-1α downstream of inflammasomes. Cell Rep. *34*, 108887.

Wang, S., Miura, M., Jung, Y.K., Zhu, H., Li, E., and Yuan, J. (1998). Murine caspase-11, an ICE-interacting protease, is essential for the activation of ICE. Cell *92*, 501–509.

Wang, Y., Li, M., Stadler, S., Correll, S., Li, P., Wang, D., Hayama, R., Leonelli, L., Han, H., Grigoryev, S.A., et al. (2009). Histone hypercitrullination mediates chromatin decondensation and neutrophil extracellular trap formation. J. Cell Biol. *184*, 205–213.

Weinrauch, Y., Drujan, D., Shapiro, S.D., Weiss, J., and Zychlinsky, A. (2002). Neutrophil elastase targets virulence factors of enterobacteria. Nature *417*, 91–94.

Wen, Z., Lei, Z., Yao, L., Jiang, P., Gu, T., Ren, F., Liu, Y., Gou, C., Li, X., and Wen, T. (2016). Circulating histones are major mediators of systemic inflammation and cellular injury in patients with acute liver failure. Cell Death Dis. *7*, e2391–e2391.

Wildhagen, K.C.A.A., De Frutos, P.G., Reutelingsperger, C.P., Schrijver, R., Aresté, C., Ortega-Gómez, A., Deckers, N.M., Hemker, H.C., Soehnlein, O., and Nicolaes, G.A.F. (2014). Nonanticoagulant heparin prevents histone-mediated cytotoxicity in vitro and improves survival in sepsis. Blood *123*, 1098–1101.

Xia, S., Zhang, Z., Magupalli, V.G., Pablo, J.L., Dong, Y., Vora, S.M., Wang, L., Fu, T.M., Jacobson, M.P., Greka, A., et al. (2021). Gasdermin D pore structure reveals preferential release of mature interleukin-1. Nature 1–5.

Xu, J., Zhang, X., Pelayo, R., Monestier, M., Ammollo, C.T., Semeraro, F., Taylor, F.B., Esmon, N.L., Lupu, F., and Esmon, C.T. (2009). Extracellular histones are major mediators of death in sepsis. Nat. Med. *15*, 1318–1321.

Xu, Z., Huang, Y., Mao, P., Zhang, J., and Li, Y. (2015). Sepsis and ARDS: The Dark Side of Histones. Mediators Inflamm. *2015*.

Yan, H., Zhou, H.F., Akk, A., Hu, Y., Springer, L.E., Ennis, T.L., and Pham, C.T.N. (2016). Neutrophil Proteases Promote Experimental Abdominal Aortic Aneurysm via Extracellular Trap Release and Plasmacytoid Dendritic Cell Activation. Arterioscler. Thromb. Vasc. Biol. *36*, 1660–1669.

Zhang, Y., Zhao, Z., Guan, L., Mao, L., Li, S., Guan, X., Chen, M., Guo, L., Ding, L., Cong, C., et al. (2014). N-acetyl-heparin attenuates acute lung injury caused by acid aspiration mainly by antagonizing histones in mice. PLoS One *9*, 97074.

Zhao, Y., Yang, J., Shi, J., Gong, Y.N., Lu, Q., Xu, H., Liu, L., and Shao, F. (2011). The NLRC4 inflammasome receptors for bacterial flagellin and type III secretion apparatus. Nature *477*, 596–602.

1508